Nonlinear Response of Deep Immersed Tunnel to Strong Seismic Shaking

Ioannis Anastasopoulos[1]; Nikos Gerolymos[2]; Vasileios Drosos[3]; Rallis Kourkoulis[4]; Takis Georgarakos[5]; and George Gazetas, M.ASCE[6]

Abstract: Critical for the seismic safety of immersed tunnels is the magnitude of deformations developing in the segment joints, as a result of the combined longitudinal and lateral vibrations. Analysis and design against such vibrations is the main focus of this paper, with reference to a proposed 70 m-deep immersed tunnel in a highly seismic region, in Greece. The multisegment tunnel is modeled as a beam connected to the ground through properly calibrated interaction springs, dashpots, and sliders. Actual records of significant directivity-affected ground motions, downscaled to 0.24 *g* peak acceleration, form the basis of the basement excitation. Free-field acceleration time histories are computed from these records through one-dimensional wave propagation equivalent-linear and nonlinear analyses of parametrically different soil profiles along the tunnel; they are then applied as excitation at the support of the springs, with a suitable time lag to conservatively approximate *wave passage* effects. The joints between the tunnel segments are modeled realistically with special nonlinear hyperelastic elements, while their longitudinal prestressing due to the great (7 bar) water pressure is also considered. Nonlinear dynamic transient analysis of the tunnel is performed without ignoring the inertia of the thick-walled tunnel, and the influence of segment length and joint properties is investigated parametrically. It is shown that despite ground excitation with acceleration levels exceeding 0.50 *g* and velocity of about 80 cm/s at the base of the tunnel, net tension and excessive compression between the segments can be avoided with a suitable design of joint gaskets and a selection of relatively small segment lengths. Although this research was prompted by the needs of a specific project, the dynamic analysis methods, the proposed design concepts, and many of the conclusions of the study are sufficiently general and may apply in other immersed tunneling projects.

DOI: 10.1061/(ASCE)1090-0241(2007)133:9(1067)

CE Database subject headings: Tunnels; Earthquakes; Dynamic analysis; Soil-structure interaction; Vibration; Nonlinear response; Seismic effects.

Introduction

In this century, more than 100 immersed tunnels have been constructed in the world for road or rail crossings (Ingerslev 1998). Typically consisting of prefabricated floatable segments 100–150 m in length, they are usually constructed in a dry-dock, made watertight with the use of special bulkheads, floated over a pre-excavated trench, and lowered with the help of special sinking rigs. The connection of two consecutive segments is performed underwater, through special rubber gaskets. Despite the necessity of specialist equipment, these tunnels have certain advantages compared to bored tunnels: They can be placed at the minimum possible depth, thus, minimizing both the imposed water-pressures and the total tunnel length; boring through relatively loose permeable soils at the sea bottom can be avoided; their construction is mostly performed ashore, ensuring high quality. The vast majority of already built immersed tunnels are located in regions of low seismicity (State-of-the-Art Report 1997). In 1997, out of 108 existing or under construction immersed tunnels, 42 were situated in the very-low-seismicity North-Western Europe, 26 in the United States of America, and 20 in Japan. In seismically active regions, earthquake loading can be critical and should be carefully taken into account (Ingerslev and Kiyomiya 1997; JSCE 1988).

The main objective of the present paper is to investigate the seismic response of a very-deep immersed tunnel, under the simultaneous action of longitudinal, transversal, and vertical seismic excitation. Emphasis is given to the consequences of *longitudinal* oscillations. This is *the* critical mode of earthquake-induced vibration, and one of the most severe loading situations for an immersed tunnel, since it may lead to decompression of the joint gaskets, jeopardizing the watertightness (and, hence, the safety) of the tunnel. Bending and shearing deformations due to lateral and vertical oscillations are not as serious a problem, since large "*shear keys*" can undertake the induced loads. A complete seismic safety evaluation of the immersed tunnel is beyond the scope of this paper.

For a proper assessment of the consequences of longitudinal and lateral vibrations, a certain degree of sophistication in our

[1]Postdoctoral Researcher, National Technical Univ., Athens, Greece.
[2]Lecturer, National Technical Univ., Athens, Greece.
[3]Graduate Research Assistant, National Technical Univ., Athens, Greece.
[4]Graduate Research Assistant, National Technical Univ., Athens, Greece.
[5]Graduate Research Assistant, National Technical Univ., Athens, Greece.
[6]Professor, National Technical Univ., Athens, Greece.

Note. Discussion open until February 1, 2008. Separate discussions must be submitted for individual papers. To extend the closing date by one month, a written request must be filed with the ASCE Managing Editor. The manuscript for this paper was submitted for review and possible publication on June 7, 2005; approved on March 5, 2007. This paper is part of the ***Journal of Geotechnical and Geoenvironmental Engineering***, Vol. 133, No. 9, September 1, 2007. ©ASCE, ISSN 1090-0241/2007/9-1067–1090/$25.00.

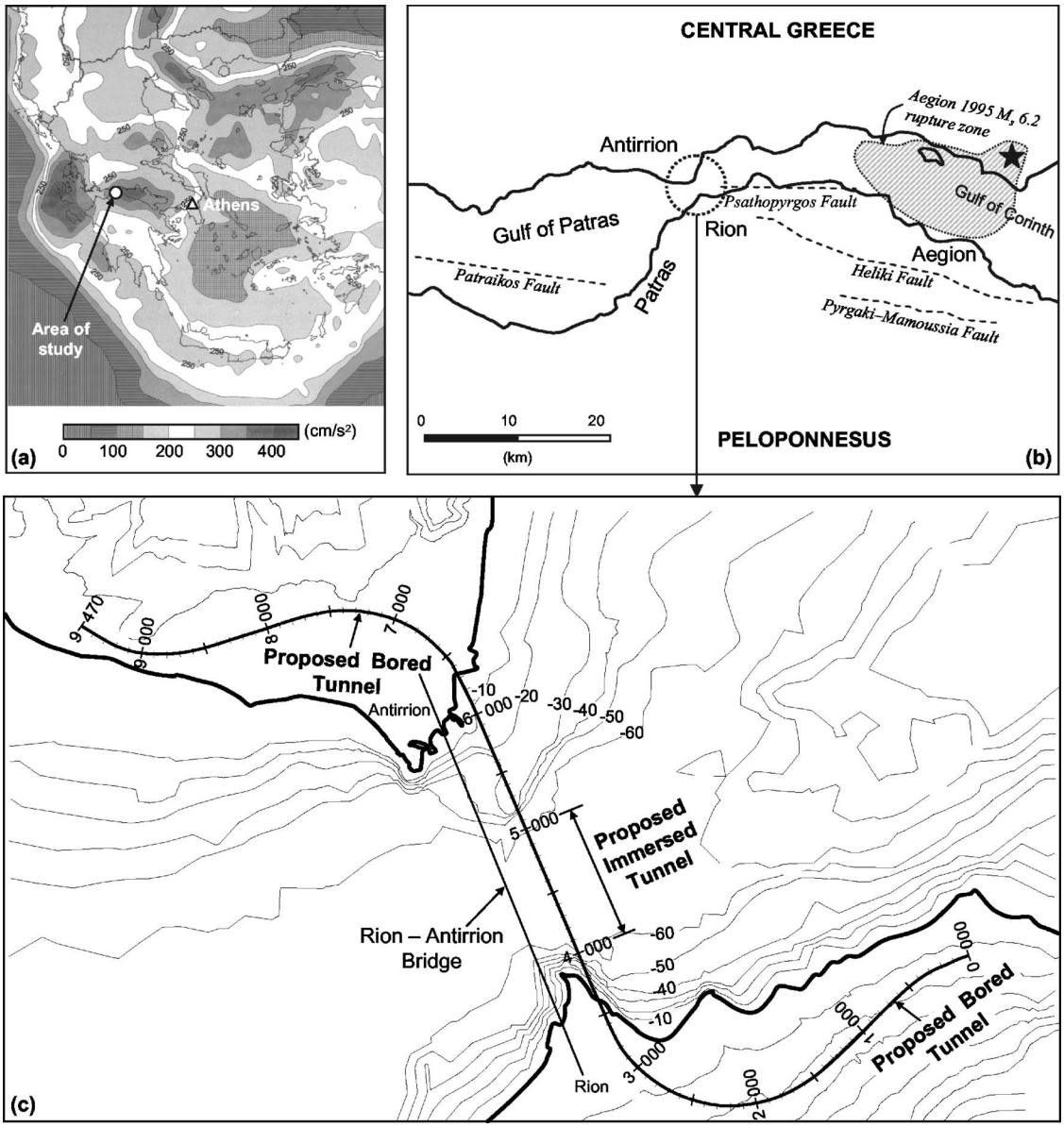

Fig. 1. (a) Seismicity map of Greece (EAK 2000); (b) major faults affecting the area of study [based on Tselentis et al. (2004), Armijo et al. (1996), and Bernard et al. (1997)]; and (c) plan view of the proposed railway link

analysis is necessary. Thus, nonlinear dynamic transient analysis of the multisegment tunnel is performed in which: (1) the behavior of the joints between segments and their longitudinal hydrostatic prestressing are modeled realistically on the basis of available (published) experimental data; (2) the interaction between the tunnel and the supporting soil is modeled with sufficient rigor, accounting for both the deformability of the soils and the ultimate behavior (sliding) at the interface; and (3) the elastic restraining at the ends of the tunnel, as well as the "allowance" for displacement in the shear keys, are modeled with realism and investigated parametrically.

The presented research is part of a feasibility study for a possible railway immersed tunnel across the Rion–Antirrion straits, in Greece. Construction of such a tunnel will constitute a major technological challenge due to the combination of great water depth (≈70 m) over its entire length, the high seismicity [Fig. 1(a and b)], and the relatively poor soil conditions. It is not in the scope of this paper to summarize a complete seismic evaluation study for this project, but merely to elucidate its seismic response and highlight the most threatening modes of vibration. Although the research for this paper was performed for the needs of this project, its methodology and conclusions may be useful in other immersed tunneling projects.

Rion–Antirrion Railway Link

The proposed railway link will connect central Greece with Peloponesus [Fig. 1(c)], crossing the Rion–Antirrion Straits, not far from the renowned recently built cable-stayed road bridge. At this narrowest point, the underwater length is 2.5 km, with a maximum depth of about 65 m, kept nearly constant over a substantial length. Two alternatives were initially investigated: (1) the solution of a bored tunnel; and (2) a hybrid solution which combines a central immersed tunnel at the deepest section of the

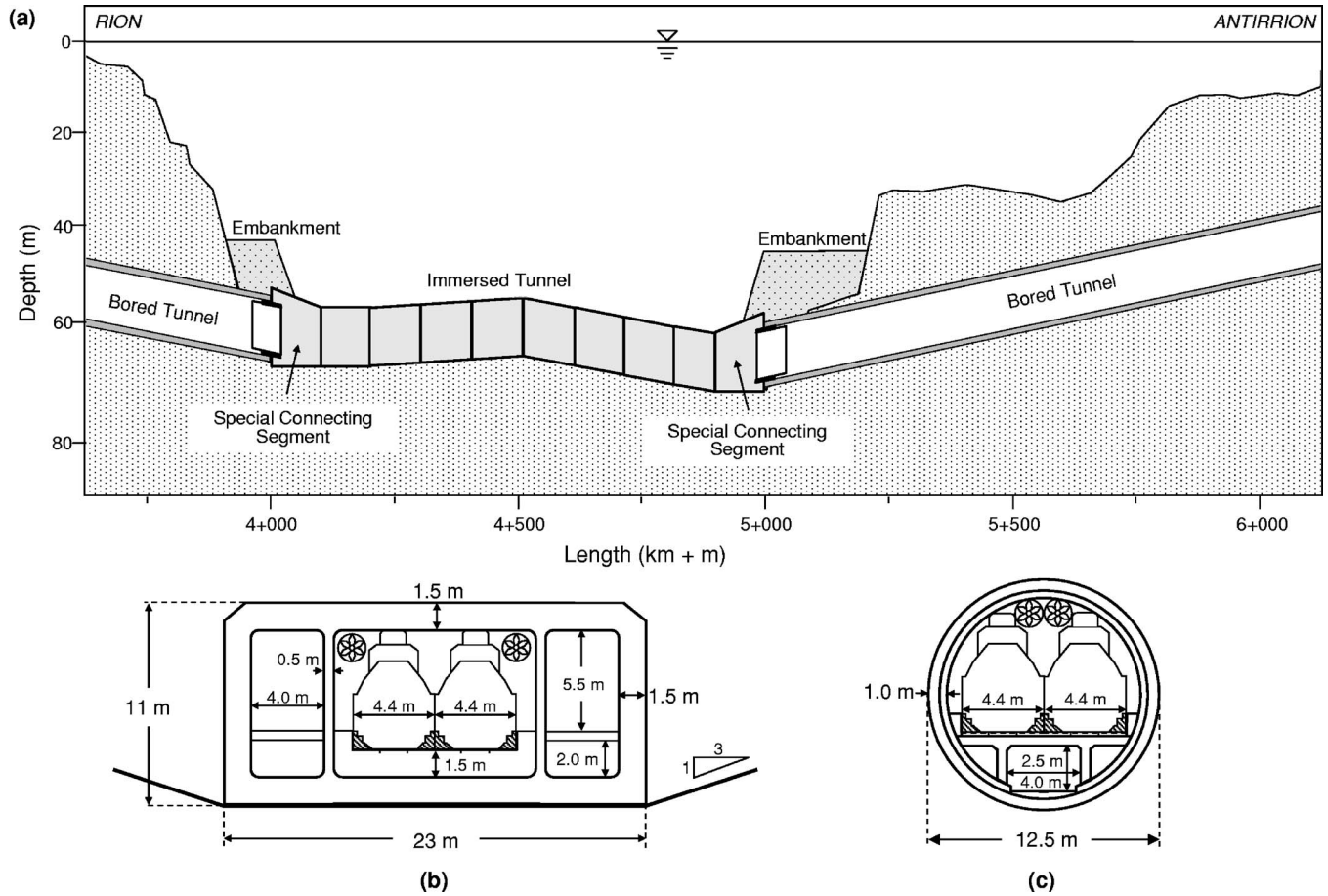

Fig. 2. (a) Longitudinal section of the proposed tunnel; (b) immersed tunnel cross section; and (c) bored tunnel cross section

crossing with two bored "approach" tunnels at the two sides.

The first solution would require boring a tunnel at 90 m depth within relatively loose (and largely permeable) soils. Facing water pressures of nearly 10 bars over a 3 km length was deemed to be too risky even with the most advanced shield tunnel boring machines (TBMs). Thus, the second solution was chosen for further study. The total tunnel length of such a solution would be 9.5 km, with the immersed part covering 980 m [Fig. 2(a)]. The cross sections of the immersed and the bored tunnel are depicted in Figs. 2(b and c). To minimize the depth (72 m), the immersed tube would not be completely embedded (as at such depths, it is not necessary to do so). Floating would be prevented by the dead load of the tunnel. Before immersion, the tube is designed to be just floatable (factor of safety against floating $F_{\text{float}} \approx 1$). Upon immersion, the segments are connected to each other and permanent concrete ballast is added to increase F_{float} to about 1.20. To this end, for a total area of the tunnel section of 261 m^2, about 20 m^3 of ballast concrete per running meter are required. In view of the small embedment, side friction is not a reliable mechanism and is, therefore, ignored.

The Rion–Antirron Straits is the narrowest crossing of the Corinthian Gulf trench, which is associated with an extensional tectonic environment in the N–S direction. With an extension rate of 8–12 mm/yr (Briole et al. 2000), it is one of the most active continental rifts on earth. It has a very high seismicity, with about 8 earthquake events of $M_s > 6$ occurring per century along its 130 km length. The strongest event of the last 50 years (Alkyonides earthquake of 1981) occurred on the eastern part of the gulf, and had a magnitude of 6.7.

The extension rate and seismicity in the western part of the gulf is somewhat lower. Faults affecting the area of study are shown in Fig. 1(b) (based on Tselentis et al. 2004, Armijo et al. 1996, and Bernard et al. 1997). Background microseismicity is very intense and concentrated within a narrow band at 6–10 km depth, dipping to the North at 15–20° (Rigo et al. 1996), indicating a deeper seismogenic fault. This has been confirmed by aftershock studies of large events, such as the 1995 Aegion earthquake (Bernard et al. 1997) [observe the projection of the 1995 rupture zone in Fig. 1(b)].

The area of study (the "Straits") has experienced five major (normal-fault) earthquakes of $M_s \approx 6$ during the last 50 years. The most recent event was the $M_s = 6.2$ Aegion 1995 earthquake, at fault distance from the Straits of about 20 km. The Straits are also affected by more distant seismic sources, such as the Ionian zone, which is by far the most active seismic zone of Greece, capable of producing earthquakes of M_s 7.5—the latest M_s 6.4 Lefkada 2003 earthquake served only as a reminder. The recently constructed Rion–Antirrion cable-stayed bridge was designed for an effective peak ground acceleration of 0.48 g. The consequences of similar strong seismic shaking are explored in this paper. The potential effects of a fault rupturing in the bedrock under the site, important as they may be, are not examined in this paper.

Utilizing extensive geotechnical exploration data obtained for the neighboring bridge, the soil stratigraphy of Fig. 3(a) was established. It consists of alternating layers of sandy-gravel to gravel, silty-sand, and clay. Soil layers near the seabed are medium-loose, not susceptible to liquefaction. The geotechnical exploration reached a maximum depth of 100 m below seabed,

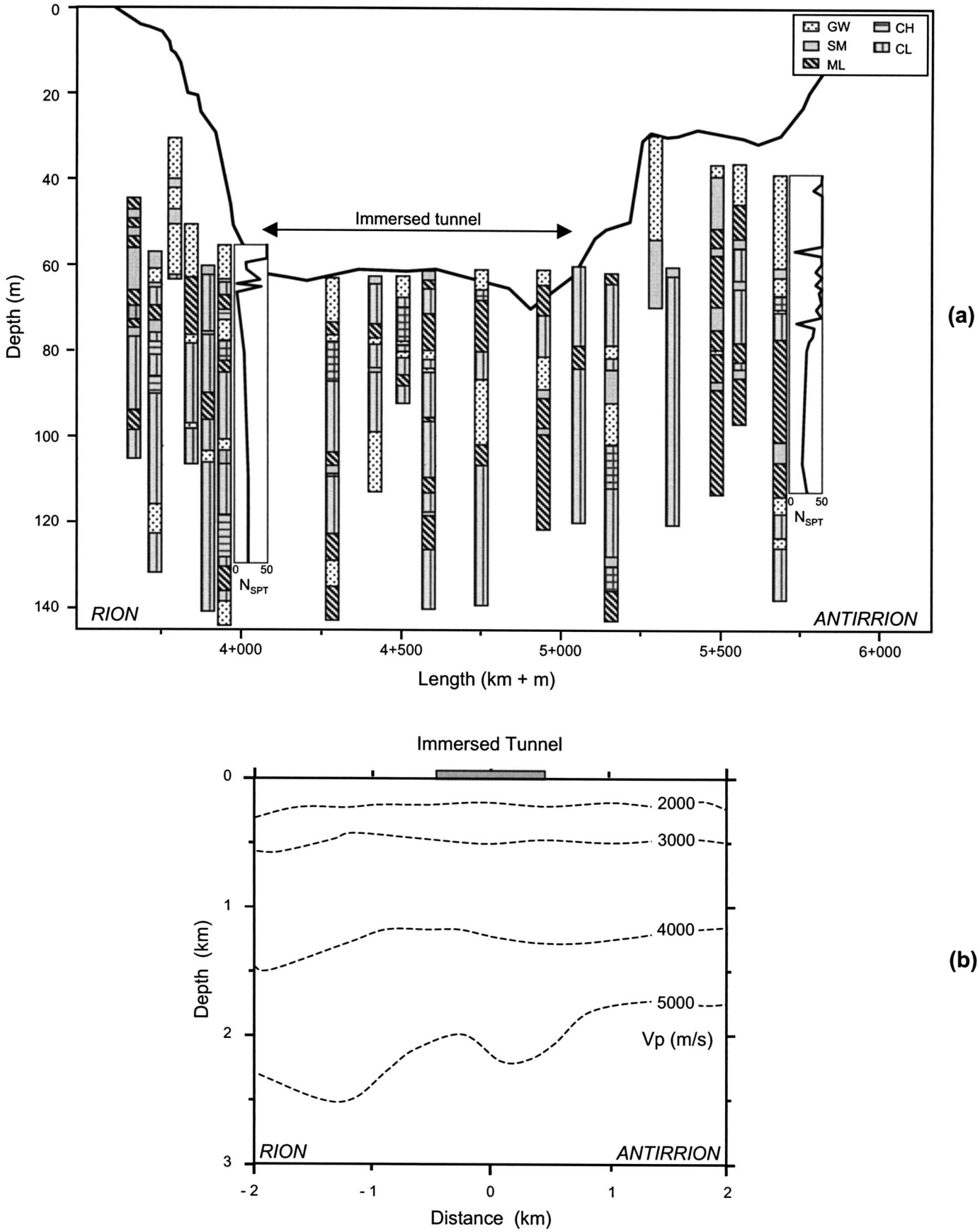

Fig. 3. (a) Compilation of geotechnical data available along a "line" 200 m east of the axis of the immersed tunnel: classification of soil layers and characteristic N_{SPT} blow counts; (b) V_p profile, based on the results of geophysical tomography in Teslentis et al. (2004)

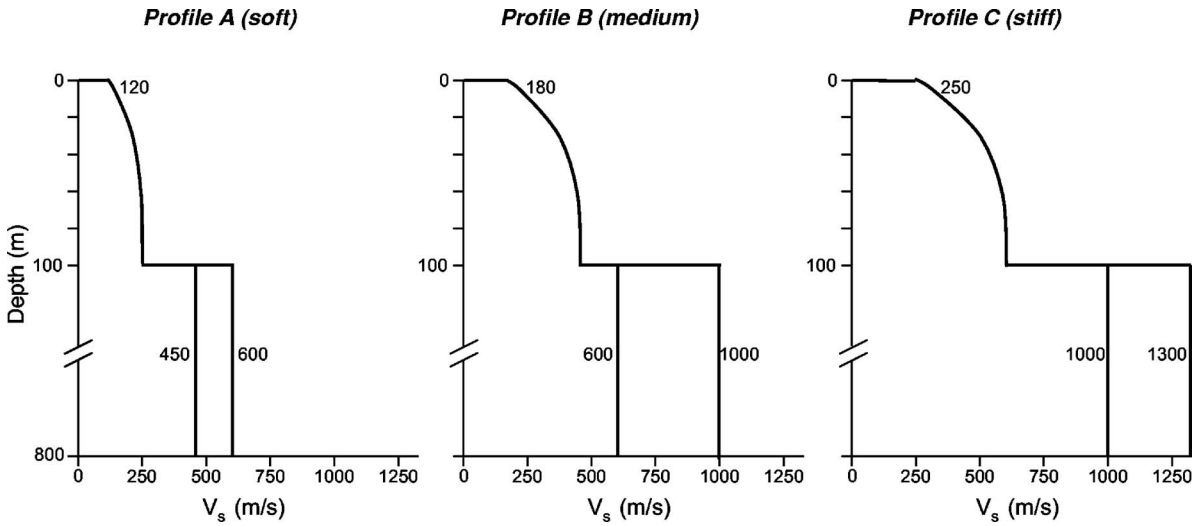

Fig. 4. Idealized shear wave velocity profiles used in the parametric investigation of soil response

without encountering bedrock. A detailed geophysical tomography conducted for the present study (Tselentis et al. 2004), gave the profile of Fig. 3(b) from which it appears that limestone bedrock ($V_p > 3{,}500$ m/s) is found at depths of the order of 800 m.

Combining such geophysical data with earlier shear wave velocity V_s measurements, three idealized ("generic") profiles were generated for the first 100 m; below this depth, V_s was varied parametrically, resulting in the six profiles of Fig. 4. Three additional profiles with no velocity contrast at 100 m depth were initially analyzed; the geophysical tomography (made available at a later stage) confirmed the range of our initial hypotheses.

Methods of Seismic Analysis of Tunnels: Brief Overview

In the absence of soil failure, slope instability, and fault-induced dislocation, the stressing of a tunnel during an earthquake arises from the displacement of the supporting ground as seismic waves arrive at the site. Two principal types of deformation incur: (1) deformation along the longitudinal axis of the tunnel, which results from both axial and curvature straining; and (2) deformation perpendicular to the tunnel axis, i.e., in the plane of the tunnel cross section. Newmark (1967), Kuesel (1969), St. John and Zahrah (1987), among others, have introduced and elaborated many of the concepts on the subject.

Axial and curvature deformations are induced by seismic wave components that propagate along the tunnel axis. For immersed tunnels, which consist of a number of nonrigidly joined segments, axial and curvature deformations impose alternating compression and extension of the joints, and this constitutes one of the most critical seismic loading situations. It is the main focus of this paper.

Seismic waves propagating perpendicularly to the tunnel axis distort the cross section of the tunnel, resulting in "ovaling" deformations of circular cross sections and "racking" deformations of rectangular cross sections (Kuesel, 1969; Owen and Scholl 1981; Merritt et al. 1985; Penzien and Wu 1998; Penzien 2000). For immersed tunnels that are not fully embedded in natural soil, as is the case here, this mode of deformation may be less critical. In any case, it is not analyzed in this paper.

To compute its response in axial and curvature deformations, the tunnel is usually approximated as an elastic beam. A complete analysis must comprise of two steps: (1) obtain the free-field deformation through wave propagation analysis; and (2) subject the soil-tunnel system to this motion. In the first step, consideration of the angle of incidence of various types of waves is necessary. Simplified harmonic wave fields in a homogeneous half-space lead to analytical closed-form expressions for longitudinal (axial and bending) strains of the ground along the tunnel. In more elaborate analyses, free-field displacement time histories are computed at certain sections along the tunnel, taking into account not only "wave passage," but, also the effect of "incoherence," which stems from the multiplicity of the angles of incidence of the seismic waves, and the randomness of wave reflections in various heterogeneities in the ground. Comprehensive reviews on the subject have been published by St. John and Zahrah (1987), Wang (1993), Power et al. (1996), and Hashash et al. (2001).

In the second step, the tunnel is supported through suitable springs, and the spatially varying motion of the first step is applied at the spring supports, thus, taking soil-structure interaction (SSI) into account through a beam-on-Winkler-foundation approach. Dynamic effects are often ignored (quasi-static solution) invoking the usually small inertia of ("embedded") tunnels (St. John and Zahrah 1987; Sakurai and Takahashi 1969; Kuribayashi et al. 1974; JSCE 1975).

Such an analysis was conducted by Hashash et al. (1998) for the retrofit of the Posey and Webster Street Tubes, connecting Alameda Island with Oakland in the San Francisco Bay. However, under strong seismic excitation, the response may be dominated by strong nonlinearities (Hashash 2000) such as the ones investigated in this paper. In such cases, dynamic analysis in the time domain is the logical solution. Acceleration time histories are applied at the supports of the soil springs, which are accompanied by relevant dashpots (Kiyomiya 1995; Hashash et al. 2001). The inertia of the tunnel may also be taken into account.

In our particular case, the inertia of the immersed tunnel may not be negligible: (1) due to the about 70 m average depth, the hydrostatic pressures are huge, resulting in a very "heavy" structure (all walls and slabs are of the order of 1.50 m in thickness); and (2) due to its only partial embedment, the overall effective inertia of the surrounding soil is not of comparable magnitude—unlike the case of bored (embedded) tunnels.

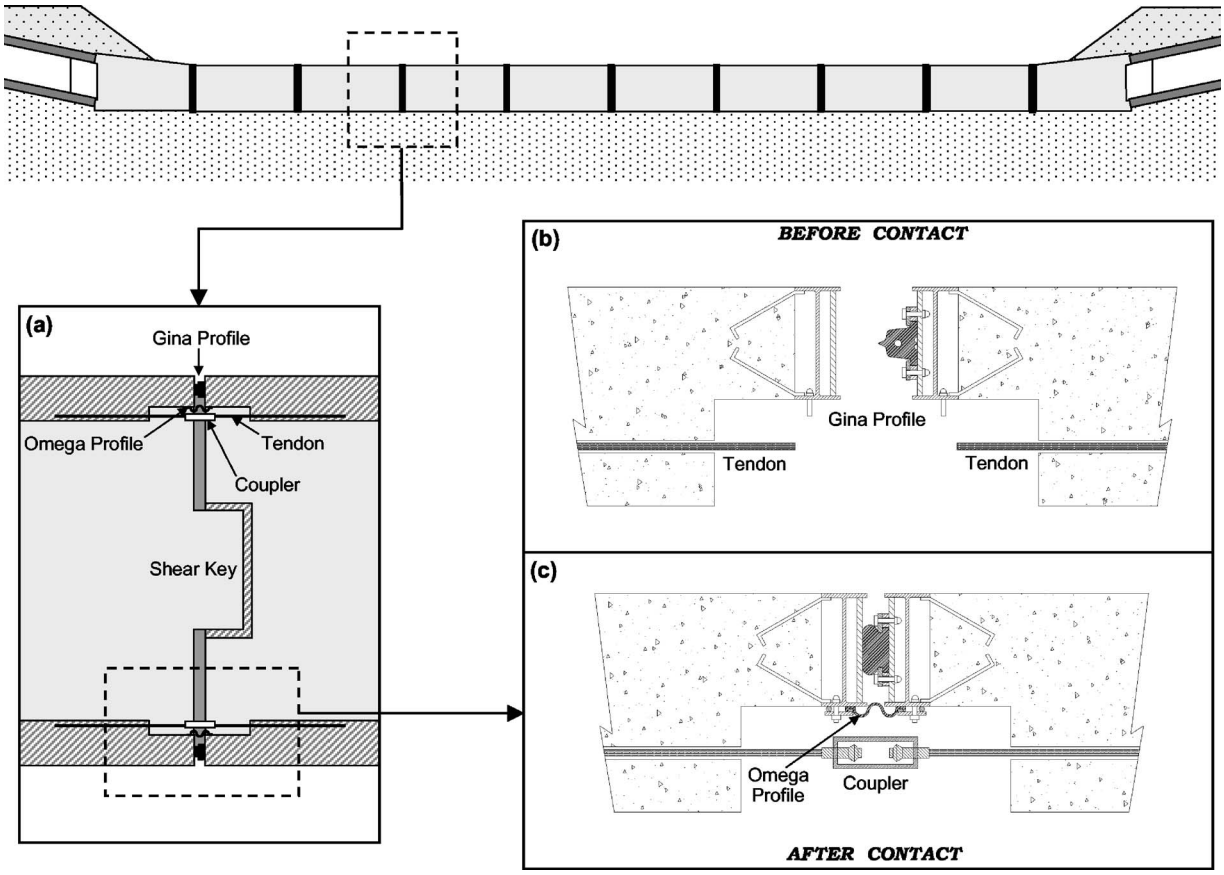

Fig. 5. Aseismic design of the immersed section of the proposed railway link: (a) schematic detail of the immersion joint, showing the Gina gasket, the omega seal, the tendons along with the couplers, and the shear key; (b) zoom-in of the immersion joint before the contact of two consecutive segments; and (c) after the compression of the Gina gasket, installation of the Omega seal and connection of the tendons with the use of a special coupler

Observed Behavior of Immersed Tunnels in Recent Earthquakes

Two immersed tunnels are known to have been subjected to moderately strong seismic shaking: (1) the Bay Area Rapid Transit (BART) tunnel in California; and (2) the Osaka South Port immersed tunnel in Japan. Both tunnels behaved very well, sustaining essentially no damage.

The BART tunnel was built in the late 1960s. With a total length of 5.8 km at 40 m maximum depth, consisting of 58 composite (exterior steel shell with reinforced concrete tube inside) segments 14.6 m wide and 6.5 in height, it had been in service for 30 years when it was shaken by the 1989 Loma Prieta M_s 7.1 earthquake. At 110 km distance from the seismogenic fault, it withstood long-period accelerations with PGA in the order of 0.20–0.30 g. It was put in service just 24 h after the earthquake. This tunnel was one of the first underground structures designed against seismic loading (Kuesel 1969). It is equipped with four special three-dimensional joints, capable of accommodating horizontal and vertical displacements of ±8 cm and ±15 cm, respectively (Douglas and Warshaw 1971; Bickel and Tanner 1982). All joints performed as expected; only a small relative displacement was noticed between the end segments and the approach structures (PB 1991).

The 1 km Osaka South Port tunnel at a 27 m depth, consisting of ten concrete segments 35 m wide and 8.6 m high, had been almost completed when it was struck by the 1995 M_{JMA} 7.2 Kobe earthquake. Located about 15 km from the seismogenic fault, this tunnel essentially experienced its *design earthquake shaking* with a recorded PGA of 0.27 g. It sustained no visible damage. In view of the failures of the embankments in the nearby Okigawa river, this success is encouraging. Tunnel segments were connected with flexible immersion joints, equipped with Gina-type rubber gaskets and secondary Omega-type waterproofing membranes. Prestressed cables and shear keys were installed to prevent excessive axial tensile and lateral shear displacements, respectively. Horizontal deformation of the joints of 2–3 cm was recorded. Neither water leakage nor structural cracking were observed. [Note in passing that it was the same earthquake that caused the most spectacular failure of an underground structure, the Daikai Metro station in Kobe (Nakamura et al. 1996), but admittedly under much stronger (by a factor of at least 3) ground shaking].

Aseismic Design of the Rion–Antirrion Immersed Tunnel

After reviewing the current aseismic design techniques, and given the satisfactory seismic performance of the Osaka South Port tunnel, a similar design was devised (Fig. 5). As already mentioned, concrete segments are constructed in a dry-dock, floated over the preexcavated trench, and lowered with the help of special sinking rigs. Each segment is lowered close to the previous one, and brought to contact under special guidance. After the two segments

gain contact, water between them is drained, and the Gina gasket is compressed by the action of the unbalanced hydrostatic pressure (acting only at the free side of the new segment) [Fig. 5(b and c)].

In our case, the hydrostatic pressure will be about 6.5 bars, necessitating the use of the largest available gasket. One problem with such a large depth is the gasket compressive loading. Given the cross-sectional area of the tunnel, 261 m^2, the total hydrostatic force acting on the gasket (before any stress relaxation) will be of the order of 174 MN ($\approx$261 $m^2 \times$ 665 kPa). For a 64 m perimeter of the gasket, the total force per running meter will be about 2.7 MPa. Under excessive *compressive* loading Gina gaskets will fail in *tension* (perpendicularly to the direction of loading). This is because rubber fails upon uniaxial compression due to tensile lateral strains (due to Poisson effect—see Kelly 1997). The largest available Gina profile might be capable of undertaking this high pressure. But, since it will be the first time for a Gina gasket to be used at such a depth, special analysis and testing are a prerequisite for acceptance.

Upon the completion of the compression phase, the secondary "Omega" seal is installed. While the Gina gasket requires a minimum compression to achieve water-tightness, the Omega seal does not. But, since none of them can transmit substantial shear or tension, shear keys and tendons are installed. A shear key at the bottom of the tunnel will transmit transverse shear forces, while two similar shear keys in the side-walls will transmit vertical shear. The tendons could transmit a limited amount of tension if necessary. It is hoped that given the initial compression of the Gina gasket, it will be unlikely for net tension to take place, as this would imply excessive decompression. In view of the anticipated strong seismic shaking, such a possibility cannot be a priori excluded; hence, the installation of tendons as a second line of defense. Tendons are connected through couplers [Fig. 5(c)], adjusted to allow some decompression before being activated.

The scope of this paper is not to present a complete seismic safety study, but only to analyze one of the critical aspects of the seismic response of the tunnel. We parametrically investigate three possible values of segment length: 70 m, 100 m, and 165 m; corresponding to the total number of immersion joints: 14, 10, and 6, respectively. The deformation of these joints, the overall resilience of the tunnel, and hence, its dynamic motion depend on this total number of joints. While the modern trend (in *nonseismic* regions) is to go for longer segments, of the order of 150–200 m, smaller lengths may be dictated by seismic considerations.

We also parametrically investigate the type of Gina gasket. The longitudinal deformation of the tunnel depends significantly on the properties of this gasket. Since it constitutes the primary seal of the tunnel, ensuring its impermeability is crucial. In longitudinal vibrations, the immersion joints are recompressed and decompressed (extension). The magnitude of such oscillatory deformation controls the design of the tendons. If decompression proves significant, the tendons will have to undertake large tensile forces to secure impermeability—an undesirable mechanism. Two types of joints are investigated [Fig. 6(a)]. Type A is the largest currently available Gina profile, the idealized behavior of which is depicted in the load-displacement backbone curve of Fig. 6(b). Kiyomiya (1995), anticipating future deeper immersed tunnels in seismically active sites, proposed and tested two alternatives: the *Horn* and the *Stirn*. Making a logical extrapolation, we anticipate a hypothetical double-size Gina gasket, denoted Type B [Fig. 6(a)], to achieve wider deformation limits, permitting significant additional recompression and decompression. The hyperelastic

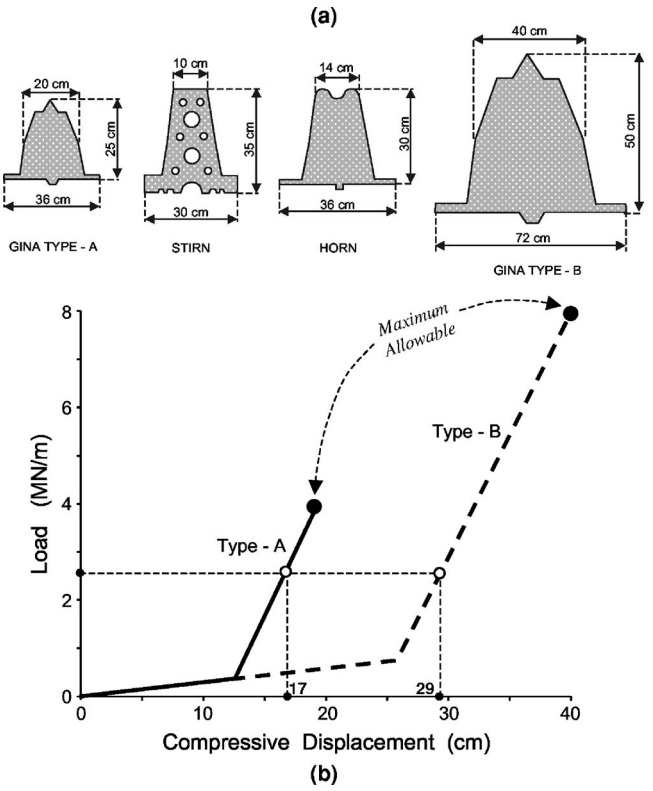

Fig. 6. (a) Geometric characteristics of existing and hypothetical joints. Beside from the widely used GINA profile, the STIRN, and the HORN have been proposed and tested by Kiyomiya (1995); (b) Hyperelastic behavior of rubber gaskets used in the analysis. Type A refers to the largest available GINA gasket, while Type B constitutes our hypothetical logical projection. The behavior has been estimated based on the half-scale tests of Kiyomiya (1995).

behavior of the two gaskets has been estimated on the basis of tests of half-sized models by Kiyomiya (1995).

Finally, we also investigate the role of the shear-key *allowance* in the transverse and vertical deformation of the tunnel. If this allowance is large enough, joints will allow relative displacement between consecutive segments. Reducing the allowance tends to make the connection more "fixed." We explore two extreme possibilities: 5 mm and 20 mm.

Dynamic Analysis Methodology

As schematically illustrated in Fig. 7, a decoupled two-step dynamic analysis methodology is applied. First, free-field acceleration time histories are computed at the base of the tunnel (seabed) through one-dimensional (1D) wave propagation analysis: (1) using the equivalent linear approximation embodied in SHAKE (Schnabel et al. 1975); and (2) applying a nonlinear inelastic constitutive model, "BWGG," developed by Gerolymos and Gazetas (2005), and encoded in NL-DYAS. Then, the computed free-field acceleration time histories are imposed on the supports of the tunnel, modeled as a multisegment beam resting on interaction springs ($\mathbf{k}$), dashpots (c), and sliders ($\boldsymbol{\mu}$).

Pertinent research results and observations from strong seismic episodes have shown that the motion may differ from one support to another, especially in the case of long structures such as tunnels. This differentiation may affect the arrival time of the seismic

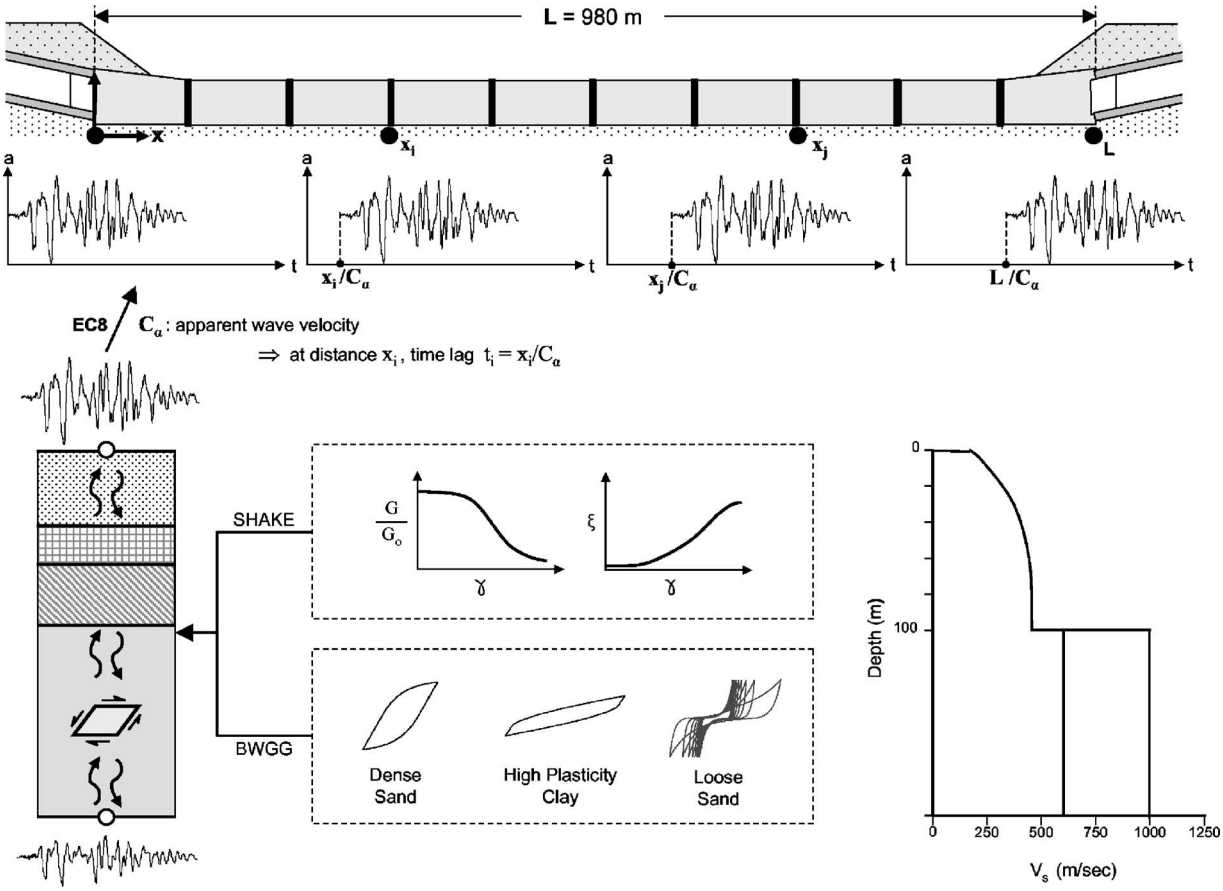

Fig. 7. Dynamic analysis methodology: the bedrock acceleration is analyzed in 1D to derive the acceleration at the seabed. Then, following the methodology of the EC8, the acceleration time histories are imposed with a time lag on the tunnel model.

waves, as well as their amplitude and frequency content. These variations are attributed to: (1) the wave passage effect (seismic waves do not propagate only vertically); (2) local soil conditions (the soil profile may vary along the alignment); and (3) random "geometric" incoherence (due to reflections, refractions, and superposition of incident seismic waves stemming from random ground heterogeneities).

To take account of the wave passage effect, we apply the methodology of Eurocode 8 (2002) and impose the acceleration time histories with a time lag; thus, asynchronous excitation of the tunnel segments is achieved. At distance x_i along the axis of the tunnel, the seismic excitation will arrive with a time lag (Fig. 7)

$$t_i = x_i/C_\alpha \tag{1}$$

where C_α=apparent wave velocity. Vertically propagating seismic shear waves would appear traveling along the ground surface (the seabed) with $C_\alpha \to \infty$. Waves propagating at incidence angle $\beta_s \neq 0°$ from the vertical, appear traveling with finite C_α

$$C_\alpha = V_s/\sin\beta_s \tag{2}$$

where V_s=shear wave velocity of the soil near the surface. The incidence angle β_s depends on the distance to the source and the ray path, but also, and crucially on the velocity contrast between the near-surface soil layers and the underlying ground. Larger contrast will lead to more intense refraction of seismic waves, and will, thus, decrease β_s.

O'Rourke et al. (1982) estimated C_α for the San Fernando (1971) and Imperial Valley (1979) earthquakes to be in the range of 2,100–5,300 m/s, with an average of 3,400 m/s. Field observations in Japan (on top of very soft soil layers) have shown that C_α may range from 1,000–2,000 m/s (Kiyomiya 1995; Okamoto 1984). Evidently, thanks to Snell's law of refraction, the apparent (S or P) wave velocity is closer to the corresponding seismic wave propagation velocity in deep rock rather than in the shallow soil (Abrahamson et al. 1991; Power et al. 1996; Hashash et al. 2001). Hence, the aforementioned high C_α values that lead to small time lags, result in more uniform motion. In our analysis, we conservatively assume C_α=1,000 m/s, in accord with the recommendations of EC8 (2002).

Regarding local soil conditions, the soil is assumed to be uniform along the tunnel—a simplification compatible with the scope of this analysis, and consistent with the "macroscopic" results of geophysical tomography (Tselentis et al. 2004) [Fig. 3(b)]. Soil conditions at the top 100 m may well turn out to be *not* completely uniform [Fig. 3(a)], and this assumption will have to be reexamined at a later stage of the project.

The effect of geometric incoherence was investigated in the early stages of our study applying the coherency loss functions of Abrahamson et al. (1991), as well as the theoretical coherency loss model of Luco and Wong (1986). In the latter case, the coherency loss function between two tunnel supports i, j is given by

Table 1. Main Seismic Sources Affecting the Area of Study [Based on Tselentis et al. (2004); Bernard et al. (1997)]

Seismic source	Length (km)	M_{max}	Strike	E-distance[a] (km)	F-distance[b] (km)	Slip Rate (mm/y)	Activity
Psathopyrgos	15.5	6.3	E-W	13	6	—	Active
Patraikos	20.0	6.3	WNW-ESE	25	12	5–8	Active
Mamoussia	18.0	6.3	WNW-ESE	35	10	0.17	Active
Heliki	35.0	6.7	WNW-ESE	30	4	1.4	Active
Aegion-1995	15.0	6.2	WNW-ESE	25	10	—	Active

[a]Epicentral distance.

[b]Distance to fault.

$$\gamma_{ij}(\omega, x_i) = \exp\left[-\left(\frac{a\omega x_{ij}}{V_s}\right)^2\right]\exp\left[-i\omega\left(\frac{x_i - x_j}{C_a}\right)^2\right] \quad (3)$$

where ω=the target frequency; and a=the incoherence factor (a measure of the loss of coherency rate with distance and frequency).

An initial sensitivity analysis was conducted to assess the effect of wave passage and geometric incoherence. Three scenarios were modeled: (1) uniform excitation; (2) wave passage effect only; and (3) wave passage effect and geometric incoherence. As expected, the differences between scenarios 1 and 2 were pronounced. In contrast, differences between scenarios 2 and 3 were negligible (less than ±10%), implying that the effect of geometric incoherence can be ignored compared to the wave passage effect. The latter is magnified with our conservative assumption of C_α =1,000 m/s.

The above are in accord with the results of numerous related studies, including Calvi and Pinto (1996) and Sextos et al. (2003 a,b) for a six span bridge subjected to asynchronous seismic excitation with parametrically variable: total length, pier stiffness, and pier-deck connection. Differences between scenarios taking account of wave passage effects *only* and the ones incorporating *both* wave passage *and* geometric incoherence effects turned out to be minor.

Seismic Environment and Selection of Ground Motions

It is not in the scope of this paper to present in detail a seismic hazard analysis of the site, but merely to highlight the methodology in selecting the ground motions for this feasibility study. The major seismogenic faults affecting the area of study have the characteristics (length L, maximum credible magnitude M_{max}, epicentral distance *E-Dist*, distance to the fault plane *F-Dist*, slip rate, and characterization) summarized in Table 1 [see also Fig. 1(b)]. The area is also affected by more distant powerful rupture zones, such as the Ionian Transformation Fault (Louvari et al. 1999). The seismic hazard was evaluated by Tselentis et al. (2004), making use of the SEISRISK III software (Bender and Perkins 1982) along with several attenuation relationships (e.g., Bozorgnia and Campbell 2004). They found for soft-rock sites that the effective ground acceleration, A, ranged from 0.20–0.33 g (at 90% nonexceedance probability in 50 years). To be consistent with the Greek Seismic Code (EAK 2000), we selected A=0.24 g for the basement (soft-rock) excitation.

To ensure that the role of the deep soil profile, as well as the consequences of near-fault directivity effects are conservatively represented in the motions to be used as ground surface excitation, the following methodology was tentatively chosen:

1. An ensemble of four recorded accelerograms which encompass a wide range of forward-rupture directivity effects, as well as number of significant cycles, form the basis of the basement excitation. They are all downscaled to peak value of 0.24 g.
2. These motions are then "propagated" through several (parametrically different) soil deposits and the resulting surface motions represent the "wave forms" of the tunnel excitation.
3. These motions are applied not simultaneously, but with a time lag, to account for wave passage effects.

Specifically, in step (a), four real earthquake records were selected (Fig. 8, Table 2): (1) the JMA record of the 1995 M_{JMA} 7.2 Kobe earthquake (Architectural Institute of Japan 1995; Nakamura et al. 1996b; Fukushima et al. 2000); (2) the Rinaldi record of the 1994 Northridge M_s 6.8 earthquake (Trifunac et al. 1998); (3) the record of the 1995 Aegion M_s 6.2 earthquake (Gazetas 1996); and (d) the record of the 2003 Lefkada M_s 6.4 earthquake (Gazetas et al. 2005; Benetatos et al. 2005).

The well-known Kobe JMA and Rinaldi accelerograms, recorded on stiff soil at *F-Dist*≈2 km, both bear the characteristics of substantial forward-rupture directivity effects (Somerville 2000; Mylonakis et al. 2006). The 1995 Aegion accelerogram was recorded also on stiff soil at *F-Dist*≈2 km [Fig. 1(b)]. The (original) record is characterized by a long-period pulse of 0.54 g, with PGV=52 cm/s, and with evidence of appreciable forward-rupture directivity effects. In view of the tectonic similarity between the Aegion region and the region of our site (only 30 km away), this record is a justified prime choice for base excitation. Finally, the Lefkada accelerogram, recorded on a medium-soft site at *E-Dist* ≈*F-Dist*≈10 km, is characterized by a sequence of eight strong motion cycles, with PGA=0.43 g and PGV=33 cm/s.

Evidently, our selection ensures that near-fault effects are given proper consideration and that the excitation is quite rich in long periods and strong pulses—important critical parameter for inelastic and sliding systems. Fling-step effects (Abrahamson 2001; Stewart et al. 2001) from potential nearby surface outbreaking faults are not considered. This is because many major seismic events of the Corinthian Gulf take place in "buried" faults that are at depths 5–10 km from the surface, dipping to the North at small angles (≈20°). Smaller faults potentially rupturing the surface of the basement rock may indeed have an effect on the tunnel structure. Such effects (ground dislocation, and fling-step affected ground shaking) are beyond the scope of this paper.

Analysis of Soil Amplification

Two types of 1D vertical wave propagation analyses were conducted: (1) applying the equivalent linear method with the SHAKE code (Schnabel et al. 1972); and (2) applying a truly

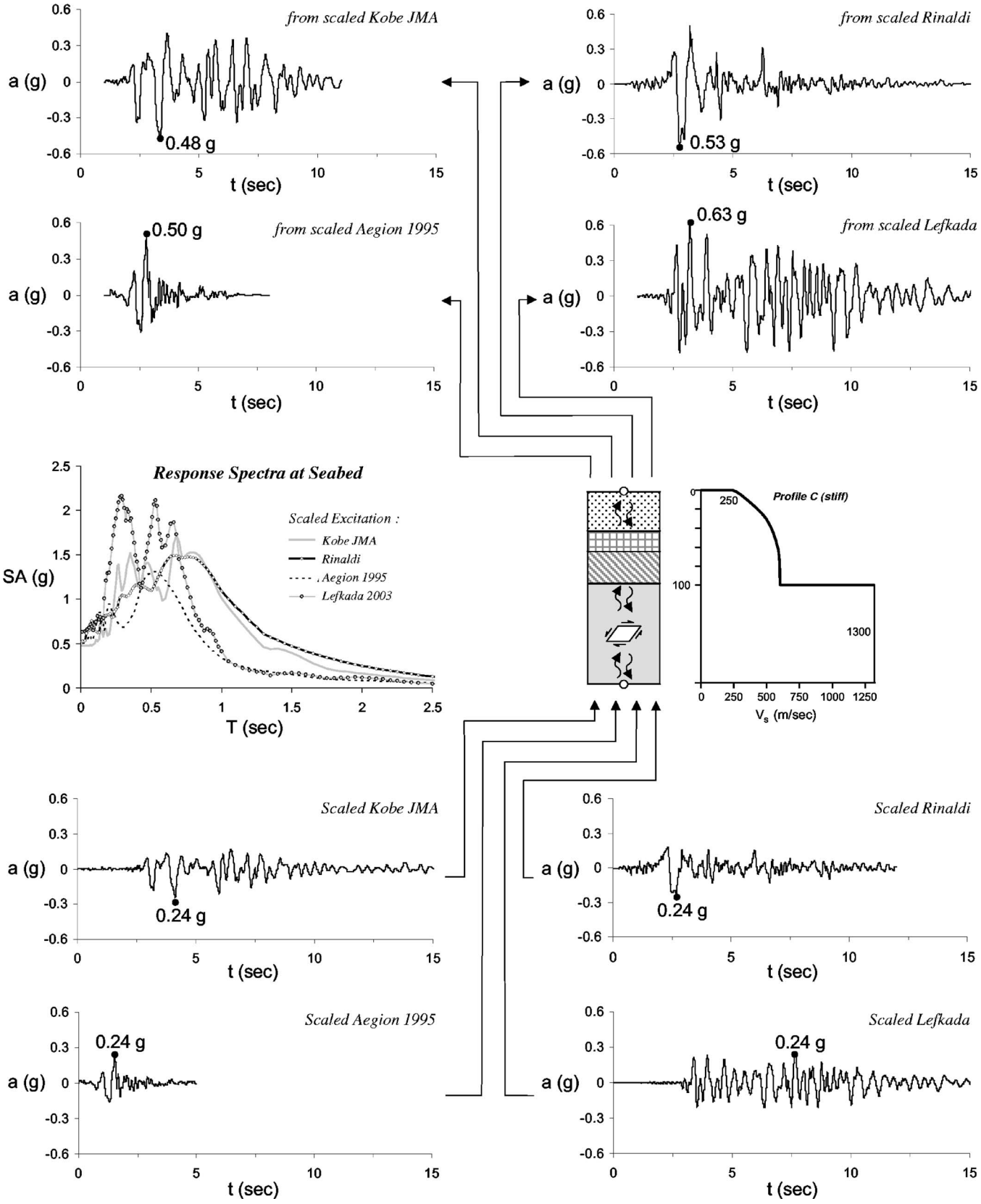

Fig. 8. 1D dynamic wave propagation analysis results (using SHAKE) for the worst-case scenario: "stiff" soil profile, with V_s=1,300 m/s below 100 m depth

Table 2. Strong Motion Records Used in the Analysis

	Record data				Original		Scaled[d]		Seabed[e]		
Record	M_s	E-Distance[a] (km)	F-Distance[b] (km)	Comp.[c]	PGA (g)	PGV (cm/s)	PGA (g)	PGV (cm/s)	PGA (g)	PGV (cm/s)	PGV[f]: PGA
Kobe JMA	7.2	22	1.5	*Long*	**0.82**	**81**	**0.24**	**24**	**0.48**	**64**	**133**
				trans	0.60	74	0.24	30	0.49	60	122
				vert	0.34	38	—	—	0.32	35	109
Rinaldi	6.8	9	2	*Long*	**0.79**	**164**	**0.24**	**50**	**0.53**	**81**	**152**
				trans	0.44	71	0.24	39	0.53	67	126
				vert	0.75	50	—	—	0.35	23	65
Aegion 1995	6.2	11	4	*Long*	**0.54**	**52**	**0.24**	**23**	**0.50**	**48**	**96**
				trans	0.49	40	0.24	20	0.48	43	90
				vert	0.20	17	—	—	0.33	28	85
Lefkada 2003	6.4	14	14	*Long*	**0.43**	**33**	**0.24**	**18**	**0.63**	**42**	**67**
				trans	0.35	26	0.24	18	0.58	37	64
				vert	0.19	11	—	—	0.40	23	58

[a]Epicentral distance.

[b]Distance to fault.

[c]Motion component.

[d]Input for 1D soil response analysis.

[e]Output from 1D soil response analysis, used as input to the tunnel-soil model.

[f]PGA (at seabed) in g, PGV (at seabed) in cm/s.

nonlinear model coded in the program NL-DYAS (Gerolymos and Gazetas 2005). The equivalent linear is definitely the most popular method, having, however, certain limitations, especially in the case of very deep soil deposits. On the other hand, most nonlinear soil models are incapable of simultaneously fitting the observed shear modulus reduction and damping curves, usually overestimating hysteretic damping at large strains (if the Masing rule is used). The recently developed NL-DYAS code uses a constitutive model that avoids such problems, and is capable of reproducing complex nonlinear characteristics of cyclic soil behavior.

Each V_s profile of Fig. 4 was analyzed using both methods (SHAKE and NL-DYAS). Thus, the uncertainty in the V_s profile below 100 m depth was investigated parametrically. For the equivalent linear method, we utilized: (1) the widely accepted modulus degradation and damping curves of Vucetic and Dobry (1991) for clayey layers; (2) the Ishibashi and Zhang (1993) relationships for sandy layers (Kramer 1996); and (3) the Laird and Stokoe (1993) curves for cohesionless soils at large depths ($>$30 m). The same data were correspondingly used for the calibration of the NL-DYAS code parameters. The calibration methodology along with an exposition of the method can be found in Gerolymos and Gazetas (2005).

1D wave propagation results (using SHAKE) for the "stiff" soil profile with V_s ($z>100$ m)=1,300 m/s (which yielded the largest soil amplification), are illustrated in Fig. 8. The downscaled (to 0.24 g PGA) records of Kobe JMA, Rinaldi, and Aegion, if applied at bedrock, produce PGAs of the order of 0.50 g at the seabed; the Lefkada record yields 0.63 g. Interestingly, the design acceleration of the neighboring Rion–Antirrion Bridge (0.48 g) was similar to the computed PGAs. The four "seabed" accelerograms of Fig. 8 were used as the input for the dynamic analysis of the tunnel.

The velocity to acceleration ratios, PGV/PGA, (in cm/s/g) of the computed seabed motions are summarized in Table 2, and compare well with those proposed by Power et al. (1996). For example, the Kobe JMA and Rinaldi records (representative of $M_s \approx 7$ earthquakes at $\leqslant$10 km distance) yield PGV/PGA ranging from 122–152. For comparison, for M_s=7.5, stiff soil conditions and site-to-source distance 20 km, Power et al. (1996) give PGV/PGA=140.

Finite-Element Modeling of the Immersed Tunnel

We utilize the finite-element (FE) code ABAQUS (2004) to perform nonlinear dynamic transient analysis of the tunnel. The FE model layout is depicted in Fig. 9. The longitudinal inclination was not taken into account, since it does not exceed 2%. Such assumption can be held to be acceptable, especially at this stage of the study. Tunnel segments are simulated using special beam elements (5 m in length) that take account of shear rigidity. Each immersion joint is modeled with two 64-node frames (one node per meter), representing the perimeter of the tube-collar connection. The 64 nodes (n1 to n64) are rigidly connected to the single *end* node (nb) of the segment beam with special transitional rigid elements, as shown in the left sketch of Fig. 9(a). Adjacent 64-node frames are connected with each other with single degree-of-freedom nonlinear springs, representing the stiffness of the joint (discussed in the sequel). All segments are connected to the soil through interaction springs and dashpots, spaced at 5 m. Since the tunnel is not completely embedded [it is practically resting on the seabed, see Fig. 2(b)], kinematic modification of inciting seismic waves is not expected to be significant and was, therefore, ignored.

The first and last segments are rigidly connected to the bored *approach* tunnels (terminal structures). The simple approximation that the bored tunnels follow the ground motion is not correct, as it ignores their bending and lateral flexibility. The assumptions of fixed supports or pinned connections at the two end segments are also incorrect. Instead, we realize that the two ends are elastically

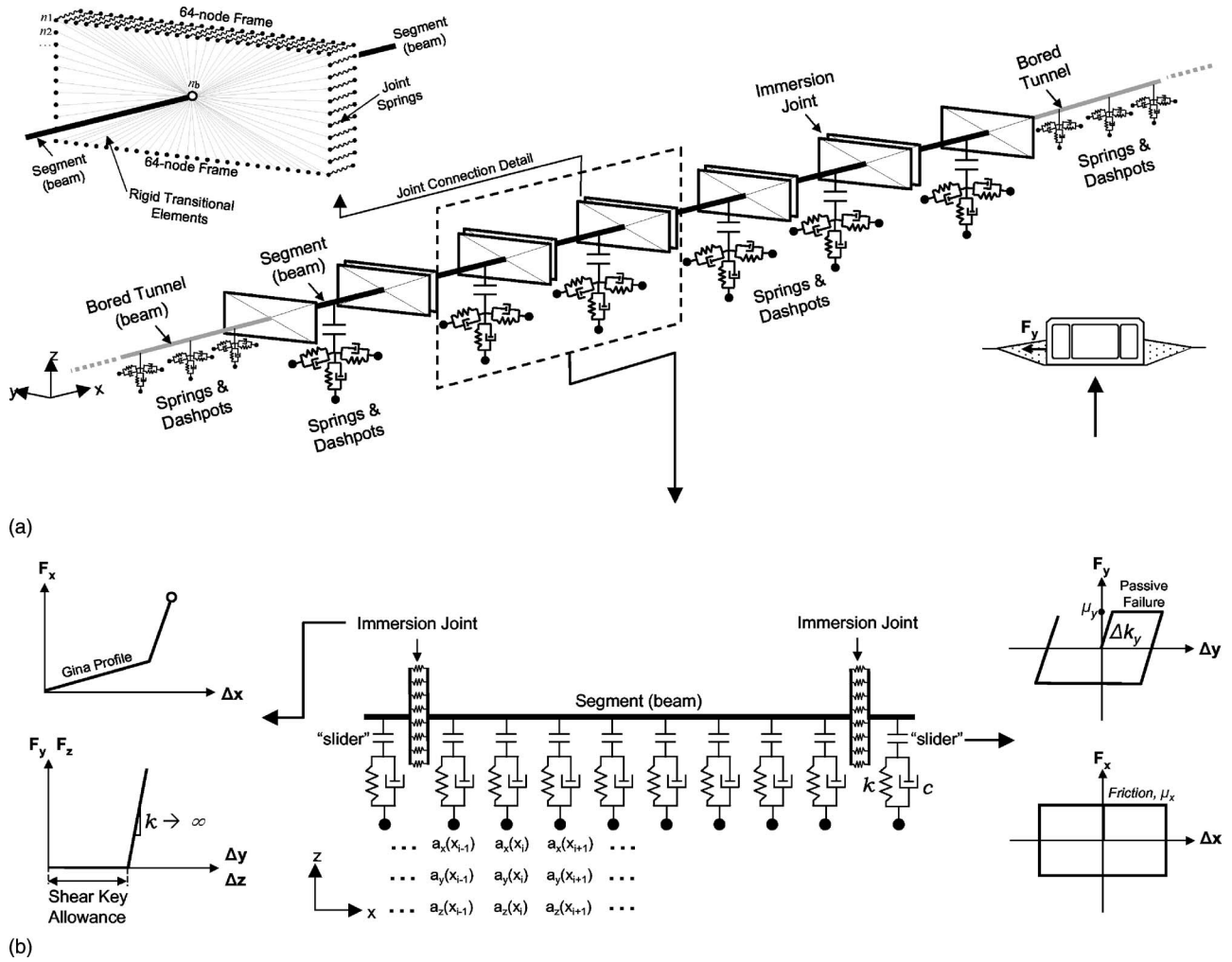

Fig. 9. Finite-element model: (a) 3-D view; (b) longitudinal section along with the force-displacement relations of the constituent elements of the model

restrained by the long circular tunnels, each of which acts as a long beam surrounded by soil. Hence, to impose the boundary conditions more realistically, the first 500 m (at each side) of the bored tunnels were incorporated in the analysis, simulated as beams on viscoelastic (Winkler) foundation. Appropriate springs and dashpots were estimated by drawing an analogy to a pile. Published elastodynamic solutions (e.g., Mylonakis 1995) were utilized to estimate distributed spring and dashpot coefficients, assuming that the "pile" (now horizontal) is embedded in a homogeneous half-space. Since the soil depth in the vicinity of the connection (60–65 m) is only five times the diameter of this pile (i.e., of the bored tunnel), spring coefficients are appropriately reduced. Moreover, radiation damping from waves originating in the pile periphery and traveling upwards would be negligible; damping coefficients were also reduced accordingly (Gazetas and Dobry 1984).

Modeling the Installation

The analysis is conducted in two stages. First, the hydrostatic pressure is applied statically to the end of each segment, to simulate the initial hydrostatic longitudinal compression. The installation procedure is simulated in detail in several steps. Starting from the left side of the model, the first segment is activated and hydrostatic pressure is applied at its right end (representing its right bulkhead). Displacement at its left end (left bulkhead) is only elastically restrained by the TBM approach tunnel. In the next step, the second segment is activated and hydrostatic pressure is deactivated from the right bulkhead of the first segment, and simultaneously applied on the right bulkhead of the second segment. The same procedure is repeated until all segments are installed. In the last step, the hydrostatic pressure is acting only on the right bulkhead of the last segment.

It is conservatively assumed that during installation, sliding on the seabed is possible: hydrostatic pressure is *not locked in by friction*. Since permanent concrete ballast is placed after installation and connection of the segments, during installation the segments are nearly "weightless" (only immersion ballast is preventing them from flotation), and, therefore, friction cannot provide substantial resistance. Hydrostatic compression is assumed to be fixed only after the tunnel is closed between the terminal structures, i.e., after the last segment is connected to the right terminal (see "State-of-the-Art Report" 1997).

After completion, the tunnel will experience some loss of its initial hydrostatic compression due to the shortening of concrete and time-dependent stress relaxation of the rubber joints. Concrete shortening is due to shrinkage and temperature effects, and

will only cause a minor loss of the initial compressive force ("State-of-the-Art Report" 1997). On the other hand, stress relaxation of rubber joints may cause significant loss. Its extent depends on the characteristics of the rubber material, such as the chemical composition (e.g., percentage of filler material) and production method (e.g., vulcanization), as well as on temperature and extent of loading (Minoura and Kamagata 1964). Given the scope of this study, such effects were not investigated in detail—the exact characteristics of the rubber (to be selected at a later stage) are not yet known.

A review of the rubber joints available in the market led to the conclusion that the total loss at the end of the lifetime of the tunnel may be in the order of 25–30%. However, considering all the conservative assumptions we have made (seismic excitation, C_α=1,000 m/s, and stiff soil profile), it would be *too conservative* to deterministically assume that all of this stress relaxation will have taken place at the time of occurrence of the maximum credible earthquake. Hence, we assume an "average" 10% loss of the initial compressive force. This relaxation is simulated in an additional static step, before proceeding to the second analysis step. At a later design stage, selection of the rubber material should be made with due consideration to its stress relaxation performance. The latter can be considerably improved with the application of prestressing (Derham 1973): Stress relaxation rate (and hence, loss of hydrostatic compression) could be reduced by one-half.

Dynamic Analysis

At the second stage of the analysis, the model is subjected dynamically to earthquake shaking. To this end, the computed acceleration time histories at seabed (Fig. 8, Table 2) are applied to the supports of springs and dashpots with the previously described time lag (modeling simply, but conservatively, the wave passage effects). All three ground motion components (a_x: Along the axis of the tunnel, a_y: Transverse, and a_z: Vertical) are included in the analysis. Initial sensitivity analysis showed that the vertical component a_z only marginally affects the results (less than ±5%). This should not be surprising: in actual strong motion records, the vertical component is of much higher frequency content than the horizontal—a fact arising from the nature of P and S waves dominating the vertical and horizontal ground motion, respectively. In mainly sliding systems, even if the vertical component of motion were (spuriously) assumed to be fully correlated (positively or negatively) with, and of the same amplitude as, the horizontal component, its effect on the response would still be negligible (Fardis et al. 2003). In our case, its only significant effect lies in the development of the bending moments M_y.

The combination of the two horizontal components (a_x and a_y) was parametrically investigated. Sensitivity analysis showed that the combination a_x=a_y=Long (where "Long" is the component with the largest PGV) maximizes the distress of the tunnel. Results presented in the sequel correspond to this conservative combination.

Soil–Tunnel Interaction Parameters

Assigning proper values to the horizontal (x,y) and vertical (z) supporting-spring constants (Winkler moduli) is a task with substantial uncertainty. For embedded tunnels, St. John and Zahrah (1987) derived an expression based on the integration of Kelvin's fundamental solution for a concentrated ("point") load acting within an infinite elastic medium (full space), assumed to be homogeneous and isotropic. Upon computing the settlement due to the load distributed uniformly across the width of the tunnel and sinusoidally over a wavelength along its axis, they derived the following approximate expression for the two horizontal spring stiffnesses [expressed as force over displacement per unit length of the tunnel (kN m m)]

$$\mathbf{k_x} \approx \mathbf{k}_y \approx \frac{16\pi(1-\nu)}{3-4\nu} G \frac{B}{\lambda} \tag{4}$$

where λ=the incident wavelength; B=the width of the tunnel; G and ν=the shear modulus and Poisson's ratio of the (homogeneous) soil, respectively. For the vertical spring stiffnesses, St. John and Zahrah (1987) utilized the fundamental solution to the problem of a surface-loaded half-space rather than of a within loaded full-space—Flamant's problem, instead of Kelvin's (see Poulos and Davis 1974; Davis and Selvadurai 1996). They thus arrived at

$$\mathbf{k_z} \approx \frac{2\pi}{1-\nu} G \frac{B}{\lambda} \tag{5}$$

The above expressions give the moduli of subgrade reaction (Winkler spring stiffnesses) as functions of the wavelength, a fact that introduces an additional uncertainty. It is interesting to note that with the ingenious introduction of the wavelength in Eqs. (4) and (5), St. John and Zahrah (1987) accomplished the circumvention of the singularity of a plane-strain solution (both *in* full space and *on* half-space).

However, with immersed tunnels: (1) the embedment is not sufficient for Kelvin's solution to even approximately apply; the half-space solutions are more appropriate; (2) the relatively high rigidity of each tunnel segment (of aspect ratio $L/B \approx 3-7$ in our study) with respect to the near-surface (usually soft) soil will lead to the deformation of the segment in horizontal translation (in the x or y direction) that may be closer to uniform than to sinusoidal; hence, the rigid-foundation solution is more appropriate; and (3) the singularity of the plane-strain solution exists only in the *static* problem, not the dynamic. One additional factor "suppresses" the singularity in this case: The soil modulus is not constant, but increases with the depth (Gazetas 1983).

Therefore, one can justifiably utilize the wealth of the published elastodynamic solutions for a rigid long rectangular foundation on half-space, to obtain not only Winkler-type springs, but also dashpots to represent the elastic soil-structure interaction. In this case, the approximate expressions for a nonhomogeneous half-space proposed by Gazetas (1991) are utilized. To this end, using as a starting point the generic profiles of Fig. 4, we eventually model the effective shear modulus profile as

$$G(z) \approx G_o \left(1 + \alpha \frac{z}{B}\right)^n \tag{6}$$

where G_o=shear modulus at z=0; $2B$=23.5 m *is* the width of the tunnel; and α, n soil model parameters. The three parameters, G_o, α, and n, were obtained by curve fitting *not* the initial $G_{\max}$ profile, but the equivalent-linear G=$G(z)$ profile, i.e., the profile of the shear modulus in the last iteration of the equivalent-linear wave propagation analysis. The distributed vertical and horizontal springs are then obtained as the static vertical, lateral, and axial stiffnesses of a very long tunnel. Expressed as stiffnesses per unit length, the Winkler moduli $\mathbf{k}_z$, $\mathbf{k}_y$, k_x, (in kN/m/m) in terms of Poisson's ratio ($\nu \approx 0.50$) are

$$\mathbf{k}_z \approx \frac{0.73}{1-\nu} G_o (1+2\alpha)^n \tag{7}$$

$$\mathbf{k}_y \approx \frac{2}{2-\nu} G_o \left(1+\frac{2}{3}\alpha\right)^n \tag{8}$$

$$\mathbf{k}_x \approx \mathbf{k}_y - \frac{0.2}{0.75-\nu}\left(1-\frac{B}{L}\right) G_o \left(1+\frac{1}{2}\alpha\right)^n \tag{9}$$

These expressions are considered valid for all frequencies—a reasonable simplification for *translational* modes of vibration (e.g., Dobry and Gazetas 1986; Gazetas 1991). Moreover, they ignore the effect of embedment; this effect is "added" indirectly only in the lateral (y) direction (Fig. 9), by increasing the spring coefficient, $\mathbf{k}_y$, by the elastic sidewall resistance

$$\Delta \mathbf{k}_y \approx E_{\text{fill}} h/2B \tag{10}$$

where E_{fill}=the (average) Young's modulus of the backfill; and h=the "effective" depth of the embedment (assumed to equal 2/3 of the actual maximum depth, 4.4 m, of Fig. 2).

A similar approach was advocated by Vrettos (2005), who also expressed the spring stiffnesses as constants, independent of wavelength or frequency. The vertical, c_z, lateral, c_y, and longitudinal, c_x, dashpot coefficients, reflecting the radiation and hysteretic damping in the soil, are similarly obtained from the expressions and diagrams of Gazetas (1991). In view of the strong soil inhomogeneity and the relatively low dimensionless frequency parameters, $a_o=(2\pi/T)B/V_{\text{so}}$, that are of prime interest here, these coefficients play a minor role in the response and are not further discussed here.

The tangential contact forces transmitted from the seabed to the tunnel are limited by friction and passive resistance. As schematically illustrated in Fig. 9, in the longitudinal direction (x) the behavior of the interface is approximated with that of a simple slider of a friction coefficient μ_x. In the transverse direction (y), the "interface" is more complex, with sliding accompanied by passive type deformation of the backfill. Therefore, the "*equivalent friction coefficient*," μ_y, is estimated through two-dimensional (2D) plane strain analysis of the tunnel cross section.

The (immersion) joints between the tunnel segments are modeled with nonlinear springs. In the longitudinal direction (x), the springs refer to the Gina gasket. As already discussed, their hyperelastic restoring force-deformation backbone curves [Fig. 6(b)] are consistent with the results of half-size model tests (Kiyomiya 1995). In the transverse (y) and vertical (z) directions Gina-type gaskets cannot transfer shear; the drift of the tunnel depends solely on the shear key allowance. Thus, the behavior of the joint is modeled with special "gap" elements, which would only transmit shear after the shear-key allowance closes, in which case, their stiffness becomes very large, depending mainly on the stiffness of the concrete section in the area of the shear key [Fig. 9(b), left].

Finite-Element Model Validation

The developed FE model was validated against simplified closed-form solutions that take account of SSI (St. John and Zahrah 1987; Sakurai and Takahashi 1969; Kuribayashi et al. 1974; JSCE 1975). Such solutions treat the tunnel-soil system as an elastic beam in elastic soil, subjected to a pseudostatic sinusoidal shear wave of wavelength λ_w and displacement amplitude D, propagating at an angle of incidence β_s in homogenous isotropic half-space (Newmark 1968; Kuesel 1969). The maximum axial force of the tunnel section $N_{\max}$ is derived considering a shear wave propagating at $\beta_s=45°$

$$N_{\max} = \frac{(\mathbf{k}_x \lambda_w/2\pi)}{1+2[(\mathbf{k}_x/E_c A_c)][(\lambda_w/2\pi)]^2} D \tag{11}$$

where E_c=Young's modulus; and A_c=cross-sectional area of the tunnel. The above expression assumes perfect bonding between tunnel and soil. The maximum bending moment of the tunnel section $M_{\max}$ is derived considering a shear wave propagating parallel to the tunnel axis

$$M_{\max} = \frac{(\mathbf{k}_y \lambda_w/2\pi)^2}{1+(\mathbf{k}_y/E_c I_c)(\lambda_w/2\pi)^4} D \tag{12}$$

where I_c=moment of inertia of the tunnel cross section.

To render our FE model comparable to the above analytical solutions, two modifications were necessary: (1) tunnel joints were replaced with beam elements (to convert the tunnel to a continuous beam); and (2) the loading (segment installation and application of hydrostatic pressure, relaxation, and seismic excitation) was replaced with a static sinusoidal wave. The latter was first assumed to incite at $\beta_s=45°$ (to compute $N_{\max}$), and then parallel to the tunnel axis (to compute $M_{\max}$), with wavelength λ_w=100 m, 200 m, and 500 m—three very severe (and rather unrealistic) cases. Perfect bonding was assumed for the tunnel–soil interface.

FE results were in accord with the aforementioned closed-form solutions [Eqs. (11) and (12)] in all cases (differences within ±13%). Even in the highly unrealistic case of λ_w=100 m, the FE model proved capable of capturing the idealized pseudostatic response. Given the 5 m spacing of tunnel supports in the FE model, only a (physically irrelevant) $\lambda_w \approx 20$ m would lead to poor results.

Dynamic Analysis Results—Effect of Segment Length

We begin by comparing the dynamic response of the tunnels with L=70 m and L=165 m. Longitudinal and transverse acceleration time histories, as well as time histories of "sliding" displacements, joint deformation, and segment internal forces are portrayed and compared in Figs. 10–13. Due to space limitation, we focus on results corresponding to the Kobe JMA-based excitation, and Type A Gina gasket combined with shear-key allowance of 5 mm.

The longitudinal $a_x(t)$ and transverse $a_y(t)$ acceleration time histories are depicted in Fig. 10. In the longitudinal (x) direction, the tunnel essentially "follows" the excitation. Increasing L only slightly increases the longitudinal acceleration on the tunnel. In the transverse direction, the response is differentiated along the length of the tunnel. At the two ends (segment B) the tunnel is forced to follow the input excitation, since it is rigidly connected to the (much stiffer) bored approach tunnels. The central part of the tunnel, however, exhibits a different behavior. With the exception of a few high-frequency acceleration "spikes" (attributable to "gapping" of the shear keys), the acceleration is cut-off at about 0.30 g ($\approx \mu_y$) implying transverse sliding.

Sliding in the longitudinal (Δ_x) and transverse (Δ_y) direction is illustrated in Fig. 11. The increase of L leads to a slight increase of Δ_x, which, however, does not exceed a mere 4 cm. There is

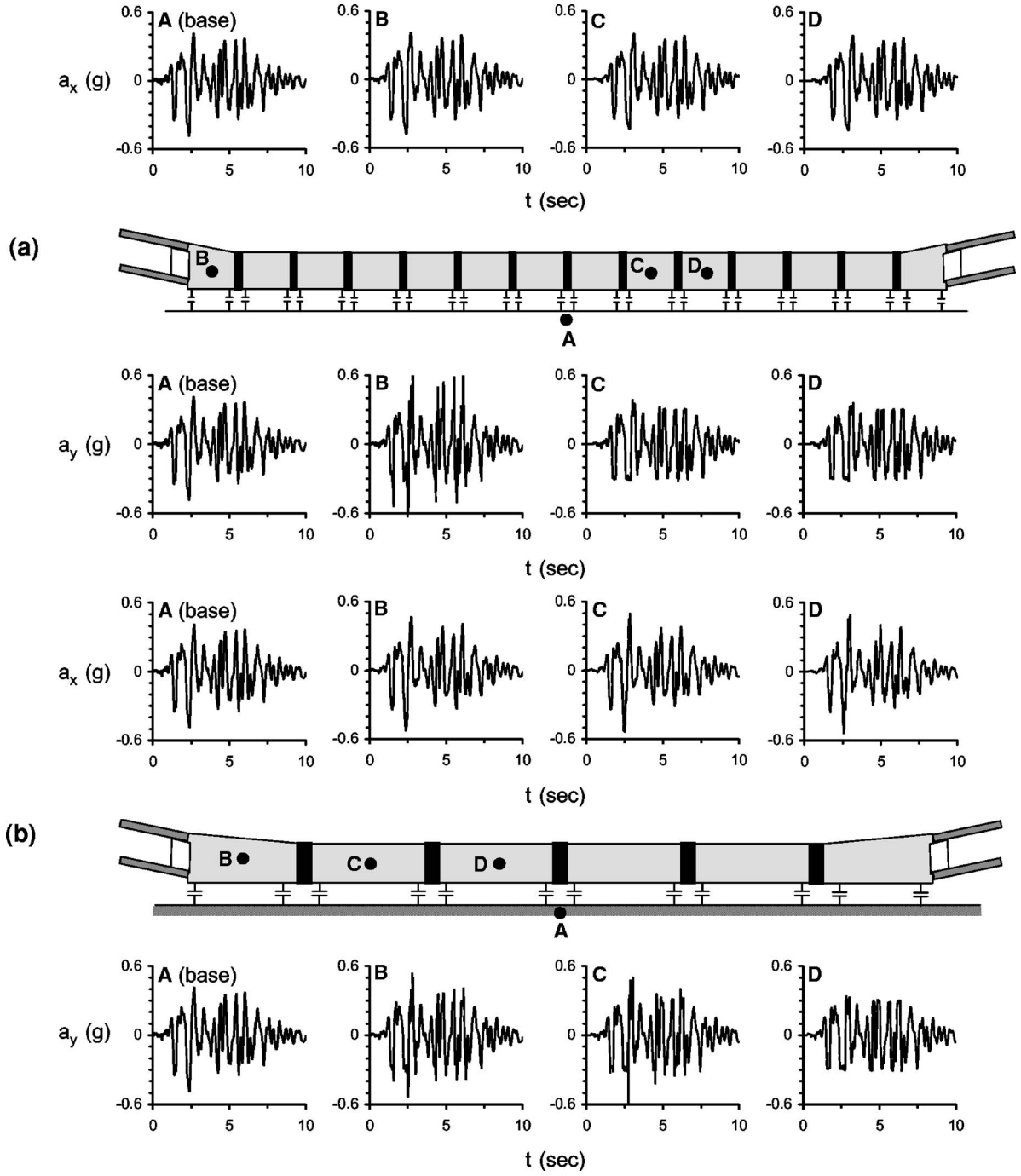

Fig. 10. Longitudinal and transverse acceleration time histories for: (a) 70 m segments; (b) 165 m segments (Kobe-JMA type excitation; Type A gasket; 5 mm shear-key allowance)

practically no permanent (residual) displacement. Sliding displacements are significantly higher in the transverse direction, with the central segments experiencing substantial sliding. The increase of L leads to a slight increase of $\Delta_{y,\max}$ In all the cases, the residual slippage does not exceed 3 cm near the center of the tunnel, being negligible at the two ends.

Deformation time histories of the immersion joints in the longitudinal (δ_x) and transverse (δ_y) direction are portrayed in Fig. 12. Recall that the longitudinal deformation is the most critical response parameter for the seismic safety of the tunnel. In that longitudinal direction, Gina gaskets experience an initial compression of about 17 cm due to hydrostatic pressure. Gasket stress relaxation over time reduces the compressive force, but not the compressive deformation of the joint. The earthquake-induced oscillation causes successive decompression and recompression of the Gina gaskets, as reflected by the fluctuations of δ_x around 17 cm. The initial compressive deformation of the joints depends on the applied hydrostatic pressure and the deformability of the rubber gasket; it is, thus, insensitive to L. However, the increase of L augments the amplitude of the dynamic fluctuations. While for $L=70$ m δ_x ranges from 12 cm (decompression) to 19 cm (further compression), increasing L to 165 m leads to $\delta_{x,\max} \approx 22$ cm and $\delta_{x,\min} \approx 10$ cm. The latter value certainly does not signal a disaster, as an ample margin is left before net tension is

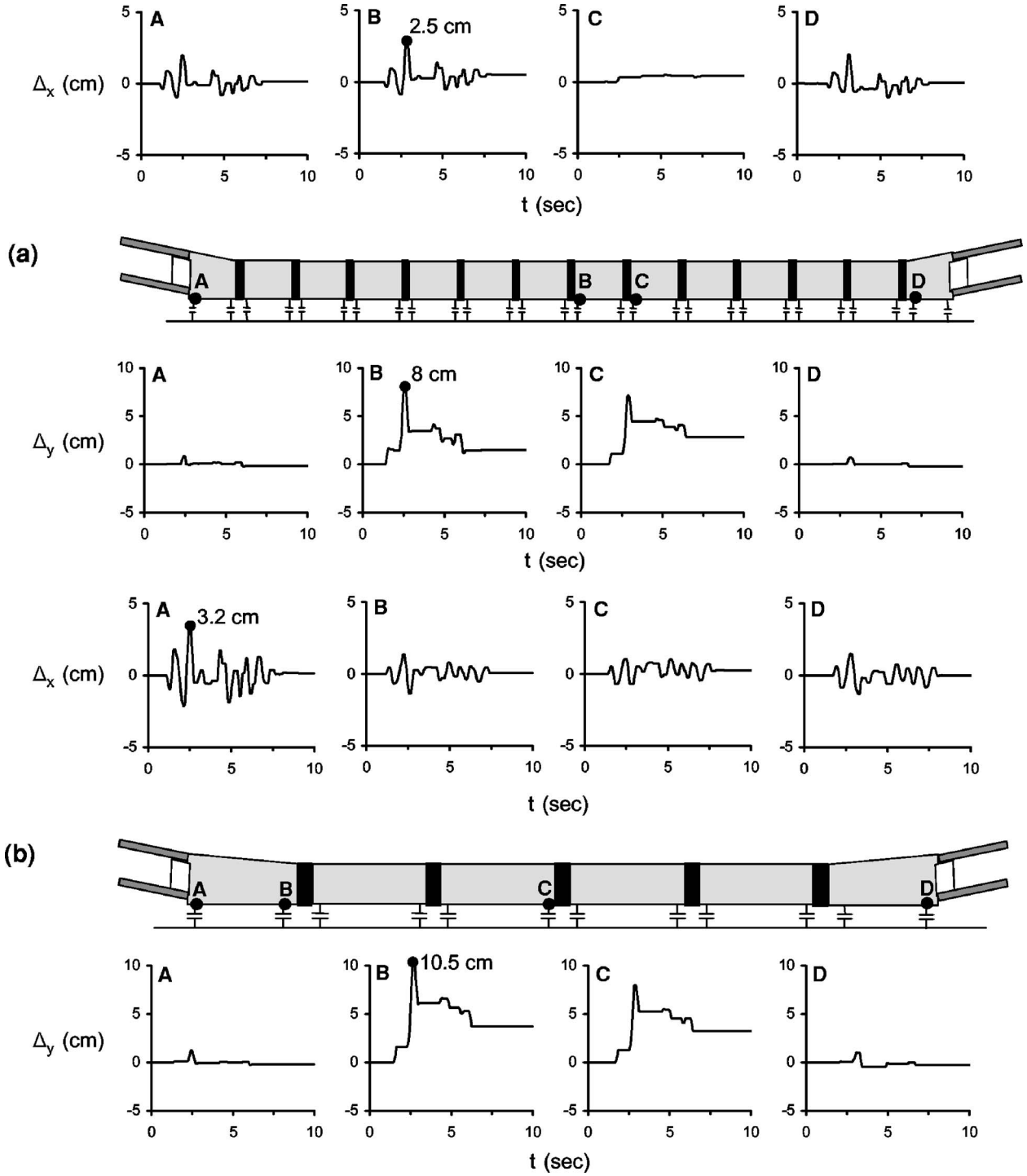

Fig. 11. Longitudinal Δx and transverse Δy sliding displacements for: (a) 70 m segments; (b) 165 m segments (Kobe-JMA type excitation; Type A gasket; 5 mm shear-key allowance)

about to develop and the tendons to engage. But going back to Fig. 6, we notice that a total dynamic compression of 22 cm exceeds the limits of the Type A gasket. The situation improves with Type B gasket. In such a case, the deformation fluctuates about a higher initial value (29 cm), reaching $\delta_{x,\max} \approx 33$ cm and dropping to $\delta_{x,\min} \approx 13$ cm: both values within acceptable limits.

In the transverse direction, the deformation of the joints mainly depends on the shear-key allowance. Interestingly, central joints experience less relative displacement than the ones near the terminals. The maximum displacement is essentially equal to the shear-key allowance (5 mm). Transverse displacements near the center never exceed 5 mm, even in the case of 20 mm shear-key allowance. The situation is different near the two terminals, where δ_y reaches 8 mm for 70 m segments. Increasing L to 165 m increases δ_y to 9 mm, indicating higher stressing of the shear-key. The δ_y that exceed the shear-key allowance represents the deformation of the concrete section. Obviously, this is just a practical approximation, only indicating the relative levels of distress of the shear-key.

Fig. 13 illustrates the bending moments M_z and axial forces N

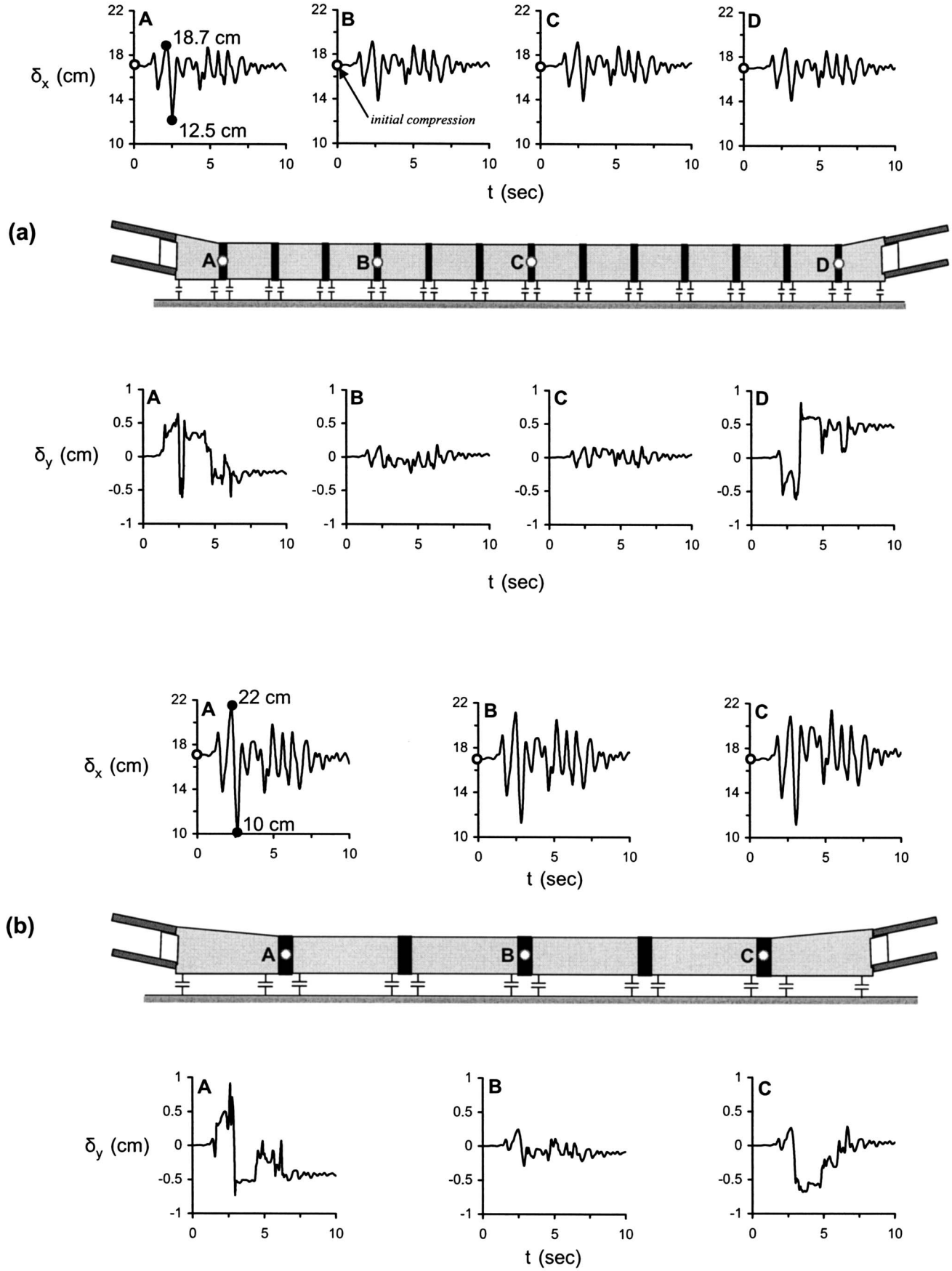

Fig. 12. Longitudinal δ_x and transverse δ_y joint deformation for: (a) 70 m segments; (b) 165 m segments (Kobe-JMA type excitation; Type A gasket; 5 mm shear-key allowance)

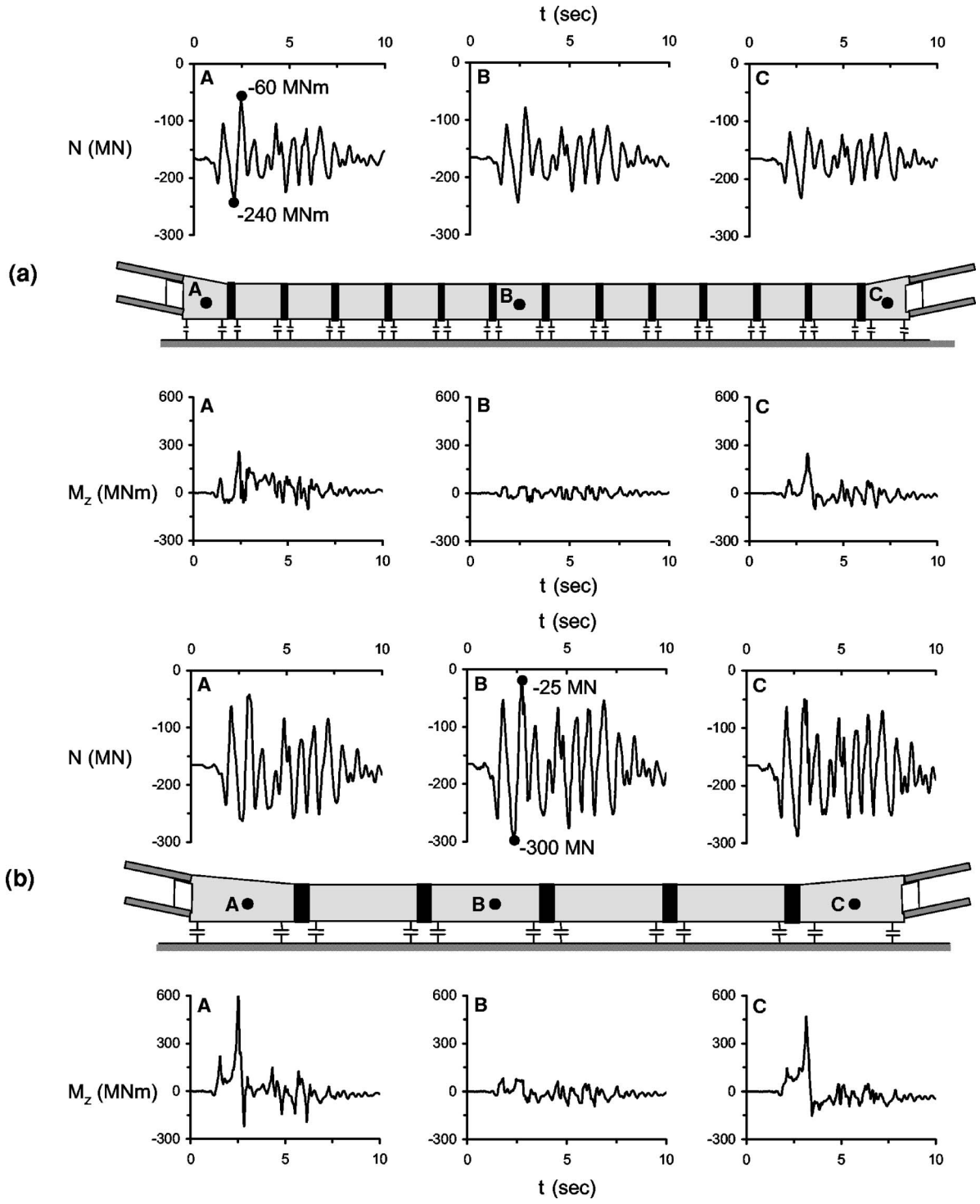

Fig. 13. Axial force and bending moment time histories for: (a) 70 m segments; (b) 165 m segments (Kobe-JMA type excitation; Type A gasket; 5 mm shear-key allowance)

in three cross sections of the tunnel. As with δ_x, N exhibits an initial (i.e., before the earthquake) "prestressing" of 157 MN from hydrostatic compression (followed by 10% stress relaxation). The minimum value of N decreases with segment length: from a comfortable 60 MN (remaining) compression for $L=70$ m, to barely 25 MN for $L=165$ m. $M_{z,\max}$ is nearly 250 MNm for $L=70$ m, increasing significantly to 600 MNm for $L=165$ m. In all examined cases, the 23.5 m $\times$ 11.2 m tunnel cross section can easily undertake the stressing.

Further Parametric Results and Discussion

A comprehensive parametric investigation has revealed that the seismic response of the immersed tunnel correlates quite well with the peak ground velocity (PGV) rather than PGA. A summary of the study is given in Figs. 14 and 15.

Specifically, Fig. 14(a) shows the dependence on PGV of the minimum and maximum longitudinal deformation experienced by any joint, $\delta_{x,\min}$ and $\delta_{x,\max}$, for the two types of Gina gasket (A, B)

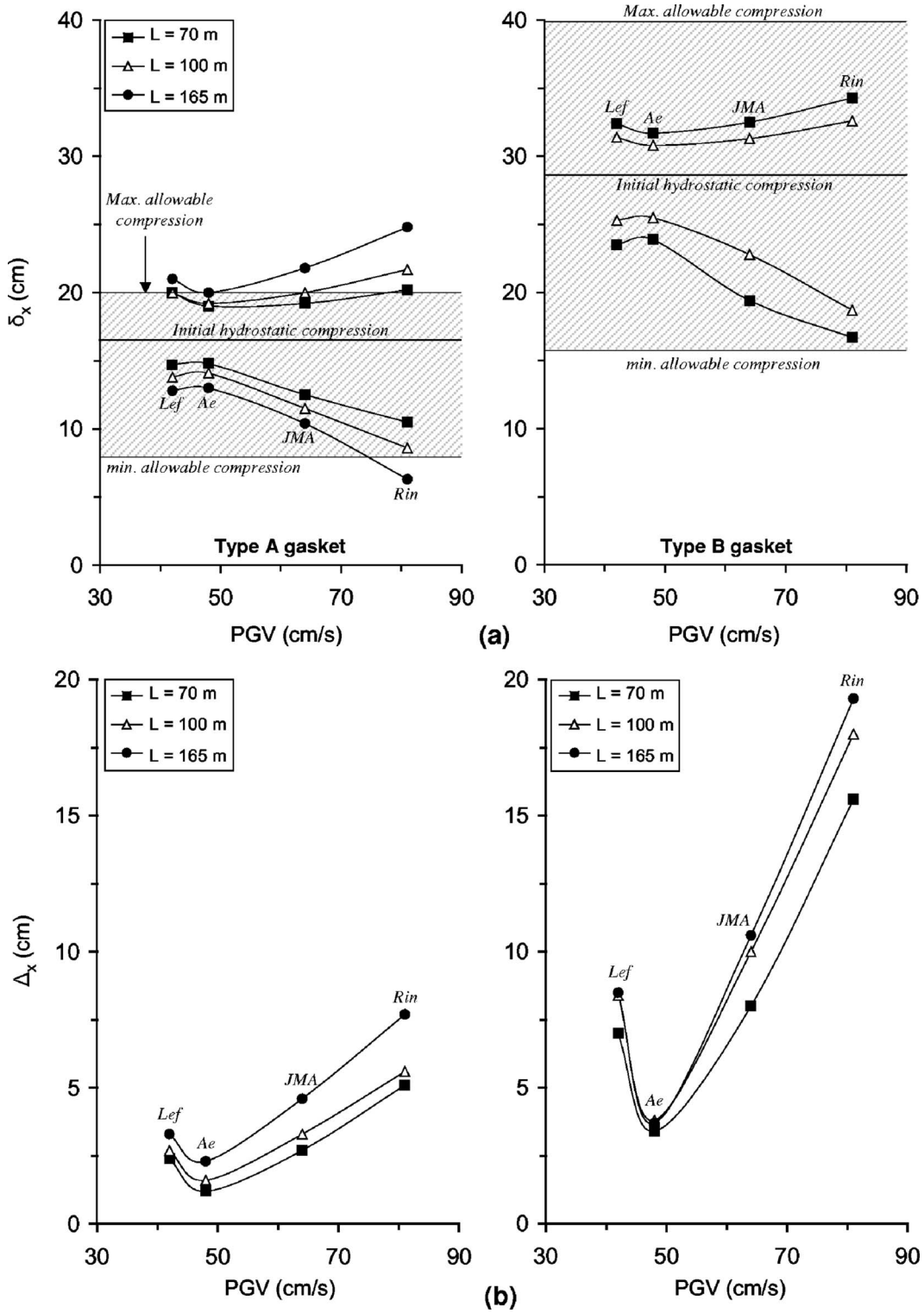

Fig. 14. Synopsis of analysis results: (a) longitudinal joint deformation δx; (b) longitudinal Δ_x and transverse Δ_y sliding displacement (*Lef:* Lefkada, *Ae:* Aegion, *JMA:* Kobe, *Rin:* Rinaldi)

and three segment lengths (70, 100, and 165 m). Also indicated in the two figures are the limiting values of the max and min compression; the former required for the safety of the gasket itself, the latter for protecting its water-tightness.

In all cases examined, $\delta_{x,\max}$ increases and $\delta_{x,\min}$ decreases, increasing PGV. The only exception is the Lefkada accelerogram, the PGV of which (42 m/s) is lower than that of Aegion (48 m/s), yet it produces larger dynamic compression and decompression of the joints. Certainly other parameters are also important: while Aegion contains a single long period acceleration pulse, Lefkada comprises several strong motion cycles (eight peaks in excess of 0.30*g* in the original record).

With $L=70$ m, both $\delta_{x,\max}$ and $\delta_{x,\min}$ are within acceptable limits even with the Type A gasket. With $L=100$ m, $\delta_{x,\max}$ exceeds

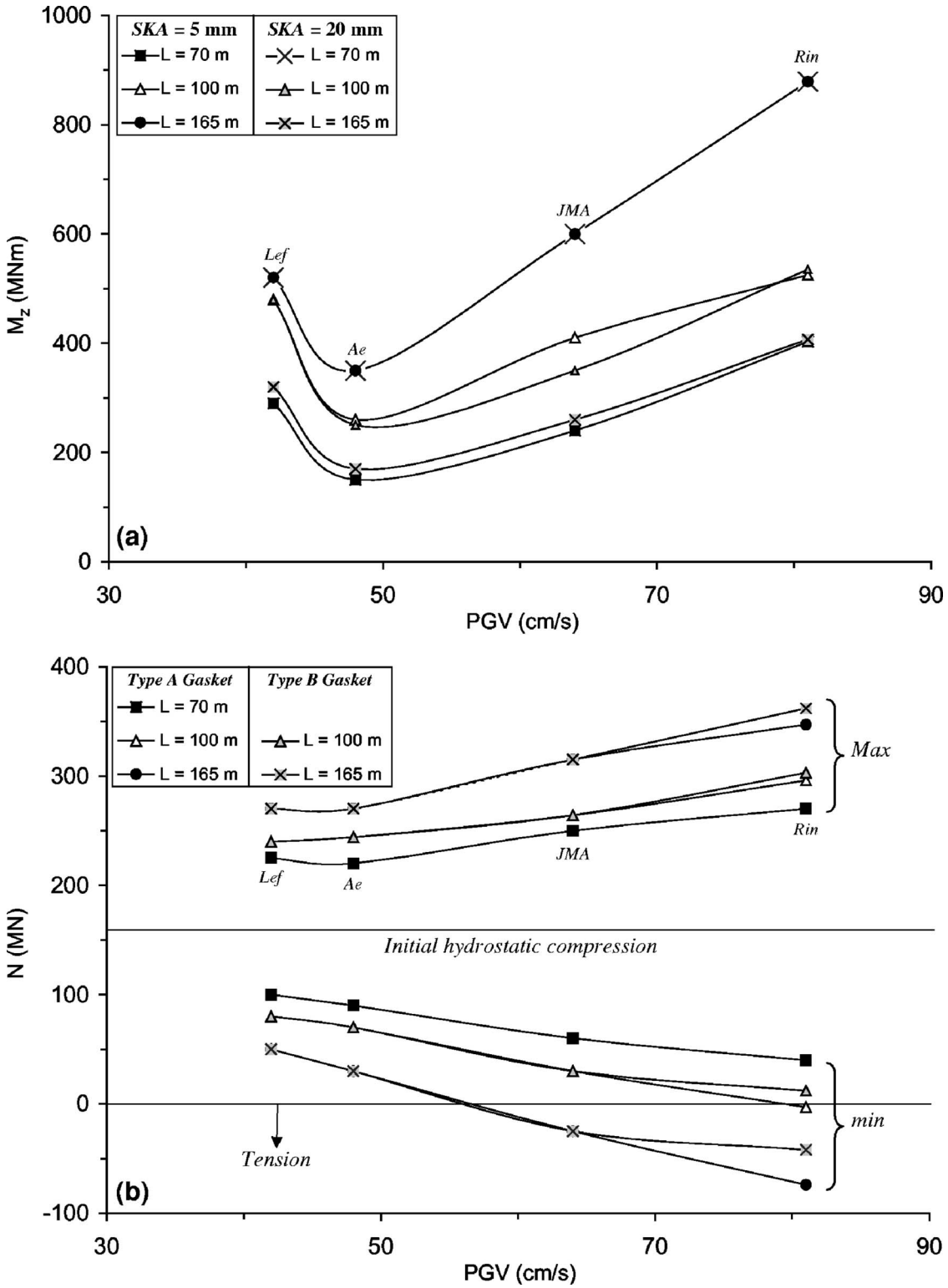

Fig. 15. Synopsis of analysis results: (a) bending moment M_z; (b) axial force N (*Lef:* Lefkada, *Ae:* Aegion, *JMA:* Kobe, *Rin:* Rinaldi)

the compression capacity of Type A gasket for PGV >65 m/s. Increasing L to 165 m, $\delta_{x,\max}$ exceeds the compression capacity of Type A gasket in all the cases, and if PGV >70 m/s, $\delta_{x,\min}$ is also reduced to "threatening" levels. With the Type B gasket, both $\delta_{x,\max}$ and $\delta_{x,\min}$ are within acceptable limits in all the cases. As expected, the shear-key allowance (SKA) does not appear to play any role (Table 3) and it is not shown as a parameter in this figure.

Fig. 14(b) plots the maximum longitudinal, Δ_x, and transverse, Δ_y, sliding displacements versus PGV. As with δ_x, with the exception of Lefkada, both Δ_x and Δ_y increase with the PGV. In all the cases, Δ_y is significantly larger (almost double) than Δ_x. The longitudinal hydrostatic prestressing of the tunnel and its end supports provide, respectively, a restoring force and a substantial constraint, which both reduce Δ_x. The hyperelastic behavior of the joints offers an additional axial restrain at large displacements.

Table 3. Synopsis of Analysis Results (Values Exceeding the Allowable Design Limits Are Denoted in Bold)

L[a] (m)	SKA[b] (mm)	GT[c]	Ecxc.[d]	PGA (g)	PGV (cm/s)	δ_x[e] (mm)		δ_y[f] (mm)		Δ_x[g] (mm)	Δ_y[h] (mm)	M[i] (MNm)	N[j] (MN)	
						min	max	min	max	min	max	max	min	max
70	5	A	*JMA*	0.48	64	125	192	−6	8	27	80	260	60	250
			Rinaldi	0.53	81	105	202	−8	8	51	156	407	40	270
			Aegion	0.50	48	148	190	−6	7	12	34	170	90	220
			Lefkada	0.63	42	147	200	−9	10	24	70	320	100	225
	20	A	*JMA*	0.48	64	125	192	−17	20	27	80	240	60	250
			Rinaldi	0.53	81	105	202	−23	22	51	158	403	39	270
			Aegion	0.50	48	148	190	−10	14	12	34	150	90	220
			Lefkada	0.63	42	147	200	−21	21	24	70	290	100	226
100	5	A	*JMA*	0.48	64	115	200	−8	8	33	100	410	30	264
			Rinaldi	0.53	81	86	**217**	−11	10	56	180	525	**−3**	296
			Aegion	0.50	48	141	192	−6	6	16	38	260	70	244
			Lefkada	0.63	42	138	200	−11	8	27	84	480	80	240
	20	A	*JMA*	0.48	64	115	200	−20	24	33	100	350	30	270
			Rinaldi	0.53	81	86	**217**	−24	24	56	182	535	**−3**	296
			Aegion	0.50	48	141	192	−15	11	16	38	250	64	246
			Lefkada	0.63	42	138	200	−24	15	27	84	480	80	240
	5	B	*JMA*	0.48	64	228	313	−8	8	33	100	410	30	264
			Rinaldi	0.53	81	187	326	−11	9	53	185	508	12	303
			Aegion	0.50	48	255	308	−6	6	16	38	260	70	244
			Lefkada	0.63	42	253	314	−11	8	27	84	480	80	240
165	5	A	*JMA*	0.48	64	104	**218**	−8	9	46	106	600	**−25**	315
			Rinaldi	0.53	81	**63**	**248**	−8	10	77	193	879	**−74**	347
			Aegion	0.50	48	130	200	−6	2	23	37	350	30	270
			Lefkada	0.63	42	128	**210**	−11	7	33	85	520	50	270
	20	A	*JMA*	0.48	64	104	**218**	−20	24	46	106	600	**−25**	315
			Rinaldi	0.53	81	**63**	**248**	22	25	77	200	879	**−74**	347
			Aegion	0.50	48	130	200	−15	2	23	37	350	30	270
			Lefkada	0.63	42	128	**210**	−17	14	33	85	520	50	270
	5	B	*JMA*	0.48	64	194	325	−8	9.0	57	106	600	**−25**	315
			Rinaldi	0.53	81	167	343	−7	10	72	193	878	**−42**	362
			Aegion	0.50	48	239	317	−6	1.5	27	37	370	30	270
			Lefkada	0.63	42	235	324	−11	6.5	34	85	520	50	270

[a]Segment length.
[b]Shear-key allowance.
[c]Gina gasket type.
[d]Excitation.
[e]Longitudinal joint deformation.
[f]Transverse joint deformation.
[g]Longitudinal sliding displacement.
[h]Transverse sliding displacement.
[i]Bending moment.
[j]Axial force.

Both Δ_x and Δ_y increase with L, but not linearly. Δ_x is more sensitive to L than is Δ_y.

The maximum bending moment M_z and axial force N are plotted in Fig. 15 versus PGV. Again, with the exception of Lefkada, M_z increases almost linearly with PGV [Fig. 15(a)]. The increase of L also causes an increase of M_z. In all examined cases, M_z can easily be undertaken by the 23.5 m × 11.2 m tunnel cross section. SKA can be seen to play a rather minor role. The increase of L makes each individual segment more flexible in the lateral sense and, thus, less sensitive to the boundary conditions at the joints. In all of the cases examined, the effect of the rubber gasket Type (A or B) is minor (Table 3).

Finally, Fig. 15(b) refers to the maximum N_{max} and minimum N_{min} axial forces. N_{max} increases almost linearly with PGV, while N_{min} decreases. The increase in L also causes an increase of N_{max} and a decrease of N_{min}. In all of the cases examined, N_{max} can easily be resisted by the A_c=261 m^2 tunnel cross section (the compressive stress never exceeds 1.5 MPa). In stark contrast, N_{min} is not always acceptable: $N_{min}<0$ implies net tension (and hence cracking of concrete). With L=70 m and 100 m, tension is

avoided in all of the cases, with a (small) exception of $N_{min} = -3$ MN in the case of Rinaldi and Type A gasket. Increasing L to 165 m makes things substantially worse: With PGV > 55 m/s, $N_{min} < 0$. The Type B gasket does improve the situation, but is not enough to completely avoid tension. Again, the response is insensitive to the SKA (Table 3).

Conclusions: Practical Aspects

The following conclusions of practical significance emerge from our study:

1. A properly designed immersed tunnel could safely resist near-fault soil-amplified strong excitation characterized by PGA as large as 0.60 g, PGV as large as 80 m/s, and containing long-period pulses.
2. The dynamically induced longitudinal deformation of immersion joints depends on the segment length L and the thickness of the Gina gasket. Since the tunnel segments are significantly stiffer than the Gina gaskets, they tend to behave as rigid blocks with most of the imposed deformation being "absorbed" in the joints. Decreasing the number of joints increases their distress.
3. For a given segment length, increasing the thickness of the Gina gasket allows for greater initial hydrostatic compressive deformation, wider deformation margins (both in decompression and recompression), and, hence, safer joint against net tension and excessive compression.
4. In the longitudinal direction, tunnel segments do not experience significant sliding over the seabed. The behavior of the system is mainly controlled by the stiffness of the Gina gaskets. Given their hyperelastic strain-stiffening characteristics, had it not been for the initial prestressing, the behavior of the tunnel would be different: Flexible joints and increased sliding.
5. In the transverse direction, the "effective" friction coefficient is enhanced by the partial backfilling of the tunnel. Nevertheless, slippage in this direction is significantly larger than in the longitudinal: Since the gaskets cannot transfer shear, there is no restoring force to limit relative deformation. In any case, sliding displacement does not exceed 20 cm, while the permanent slippage is much less (<8 cm).
6. It appears feasible to design and construct an immersed tunnel at a great depth (≈ 70 m). Dredging at such a depth can be accomplished with modern equipment. Boring of the approach tunnels under pressures of 6.5 bars is also manageable. This study has explored and to an extent proved the seismic feasibility of the project. The construction itself of the proposed rail link (when approved and financed) will constitute a great technological challenge.

Limitations

The conclusions of this study are valid, with certain "theoretical" limitations:

1. The effect of heterogeneous local soil conditions and ground motion incoherency have not been examined in this study (the subsoil was assumed to be uniform along the immersed tunnel). Although this is consistent with the results of geophysical tomography, such effects may be important and should be examined carefully in the final design stage.
2. The effect of time-dependent rubber gasket stress relaxation was not investigated in detail. Such relaxation can cause a loss of the initial hydrostatic compressive force of the order of 25%–30%. In this study, only an average 10% loss was assumed.
3. The effect of tectonic displacements from a normal fault rupturing under the site has not been investigated in this paper (it belongs to a future publication). Such displacements *may play* a major role in the feasibility of the project as they produce permanent tensile deformation, effectively reducing the hydrostatic compression of the joints, and rendering the tunnel more vulnerable to future seismic oscillations.

Acknowledgments

The writers would like to acknowledge the financing of this research project by the Greek Railway Organization. The third writer (V. D.) would also like to acknowledge the State Scholarships Foundation of Greece (IKY) for financial support. We also thank Hans van Italie, Hendrik Postma, Gerard H. van Raalte, P. van der Burg, and Royal Boskalis S.A. for kindly offering their comments and suggestions on construction-related issues. Our "computational" belief on the feasibility of the project was greatly enhanced by their real life experience. Finally, the writers would also like to acknowledge the anonymous reviewers who played a significant role in shaping and improving the manuscript.

References

ABAQUS, Inc. (2004). *ABAQUS V.6.4 user's manual*, Providence, R.I.

Abrahamson, N. A. (2001). "Near fault ground motions." ⟨http://civil.eng.buffalo.edu/webcast/Abrahamson/presentation⟩.

Abrahamson, N. A., Schneider, J. F., and Stepp, J. C. (1991). "Empirical spatial coherency functions for soil-structure interaction analyses." *Earthquake Spectra*, 7(1), 1–27.

Architectural Institute of Japan. (1995). *Strong motion records of the Hyogo-ken Nanbu Earthquake* (in Japanese).

Armijo, R., Meyer, B., King, G., Rigo, A., and Papanastassiou, D. (1996). "Quaternary evolution of the Corinth rift and its implications for the late Cenozoic evolution of the Aegean." *Geophys. J. Int.*, 126, 11–53.

Bender, B., and Perkins, D. (1982). "SEISRISK II. A computer program for seismic hazard estimation." *USGS Open File Rep.*, *USGS*, 82–293.

Benetatos, C., et al. (2005). "The 14 August 2003 Lefkada Island (Greece) earthquake: Focal mechanisms of the mainshock and of the aftershock sequence." *J. Seismol.*, 9(2), 171–190.

Bernard, P., et al. (1997). "The M_s=6.2, June 15, 1995 Aigion earthquake (Greece): Evidence for a low-angle normal faulting in the Corinth rift." *J. Seismol.*, 1, 131–150.

Bickel, J. O., and Tanner, D. N. (1982). "Sunken tube tunnels in: Tunnel engineering handbook." J. O. Bickel and T. R. Keusel, eds., Van Nostrand Reinholds, Chap. 13, 354–394.

Bozorgnia, Y., and Campbell, K. W. (2004). "Engineering characterization of ground motion." *Earthquake engineering*, Y. Bozorgnia and V. V. Bertero, eds., Chap. 5, CRC, Boca Raton, Fla.

Briole, P., et al. (2000). "Active deformation of the Corinth rift, Greece: Results from repeated global positioning surveys between 1990 and 1995." *J. Geophys. Res.*, 105, 25,605–25,625.

Calvi, M., and Pinto, P. (1996). "Experimental and numerical investigations on the seismic response of bridges and recommendations for code provisions." *Prenormative Research in Support of Eurocode 8, Rep. 4*, European Consortium of Earthquake Shaking Tables.

Davis, R. O., and Selvadurai, A. P. S. (1996). *Elasticity and geomechanics*, Cambridge University Press, Cambridge, U.K.

Derham, C. J. (1973). "Creep and stress relaxation of rubbers—The effects of stress history and temperature changes." *J. Mater. Sci.*, 8, 1023–1029.

Dobry, R., and Gazetas, G. (1986). "Dynamic response of arbitrarily-shaped foundations." *J. Geotech. Engrg.*, 112, 109–135.

Douglas, W. S., and Warshaw, R. (1971). "Design of seismic joint for San Francisco Bay Tunnel." *J. Struct. Div.*, 97(4), 1,129–1,141.

EAK. (2000). *Greek seismic code*, O.A.S.P., Athens, 2001 (in Greek).

EC8. (2002). "Design of structures for earthquake resistance." European Committee for Standardization (CEN), *Eurocode 8*, Brussels.

Fardis, N., Georgarakos, P., Gazetas, G., and Anastasopoulos, I. (2003). "Sliding isolation of structures: Effect of horizontal and vertical acceleration." *Proc., FIB Int. Symp. on Concrete Structures in Seismic Regions*, Athens, Greece.

Fukushima, Y., Irikura, K., Uetake, T., and Matsumoto, H. (2000). "Characteristics of observed peak amplitude for strong ground motion from the 1995 Hyogoken Nanbu (Kobe) earthquake." *Bull. Seismol. Soc. Am.*, 90, 545–565.

Gazetas, G. (1983). "Analysis of machine foundation vibrations: State of the art." *Int. J. Soil Dyn. Earthquake Eng.*, 2(1), 2–43.

Gazetas, G. (1991), *Foundation vibrations: Foundation engineering handbook*, 2nd Ed., H. Y. Fang, ed., Kluwer, Dordrecht, Chap. 15, 553–593.

Gazetas, G. (1996), *Soil dynamics and earthquake engineering: Case histories*, Symeon, Athens (in Greek).

Gazetas, G., Anastasopoulos, I., and Dakoulas, P. (2005). "Failure of harbor quaywall in the Lefkada 2003 earthquake." *Proc., of Geotechnical Earthquake Engineering Satellite Conf.—Performance Based Design in Earthquake Geotechnical Engineering: Concepts and Research*, 62–69.

Gazetas, G. and Dobry, R. (1984). "Horizontal response of piles in layered soils." *J. Geotech. Engrg.*, 110, 20–40.

Gerolymos, N., and Gazetas, G. (2005). "Constitutive model for 1-D cyclic soil behavior applied to seismic analysis of layered deposits." *Soils Found.*, 45(3), 147–159.

Hashash, Y. M. A. (2000). "Seismic behavior of underground structures and site response." *Proc., of the China-U.S. Millennium Symp. of Earthquake Engineering: Earthquake Engineering Frontiers in the New Millennium*, 8–11.

Hashash, Y. M. A., Hook, J. J., Schmidt, B., and Yao, J. I.-C. (2001). "Seismic design and analysis of underground structures." *Tunn. Undergr. Space Technol.*, 16(2), 247–293.

Hashash, Y. M. A., Tseng, W. S., and Krimotat, A. (1998). "Seismic soil-structure interaction analysis for immersed tube tunnels retrofit." *Proc., Geotechnical Earthquake Engineering and Soil Mechanics III 2*, Geotechnical Special Publication, No. 75, ASCE, Reston, Va., 1380–1391.

Ingerslev, L. C. F. (1998). "Water crossings—The options." *Tunn. Undergr. Space Technol.*, 13(4), 357–363.

Ingerslev, C., and Kiyomiya, O. (1997), "Earthquake analysis, immersed, and floating tunnels." *Working Group Report, ITA*, 2(2), 76–80.

Ishibashi, I. and Zhang, X. (1993). "Unified dynamic shear moduli and damping ratios of sand and clay." *Soils Found.*, 33(1), 182–191.

JSCE. (1975). "Specifications for earthquake resistant design of submerged tunnels." Japanese Society of Civil Engineers, Tokyo.

JSCE. (1988). "Earthquake resistant design for civil engineering structures in Japan." Japanese Society of Civil Engineers, Tokyo.

Kelly, J. M. (1997). *Earthquake resistant design with rubber*, 2nd Ed., Springer, N.Y.

Kiyomiya, O. (1995). "Earthquake-resistant design features of immersed tunnels in Japan." *Tunn. Undergr. Space Technol.*, 10(4), 463–475.

Kramer, S. L. (1996). *Geotechnical earthquake engineering*, Prentice-Hall, England Cliffs, N.J.

Kuesel, T. R. (1969). "Earthquake design criteria for subways." *J. Struct. Div.*, 6, 1213–1231.

Kuribayashi, E., Iwasaki, T., Kawashima, K. (1974). "Dynamic behavior of a subsurface tubular structure." *Proc., 5th Symp. on Earthquake Engineering*, India.

Laird, J. P., and Stokoe, K. H. (1993). "Dynamic properties of remolded and undisturbed soil samples tested at high confining pressures." *Geotechnique Engineering Rep. GR93-6*, Electric Power Research Institute.

Louvari, E., Kyratzi, A., and Papazachos, B. (1999). "The Cephalonia transform fault and its extension to western Lefkada Island." *Tectonophysics*, 308, 223–236.

Luco, J. E., and Wong, H. L. (1986). "Response of a rigid foundation to a spatially random ground motion." *Earthquake Eng. Struct. Dyn.*, 14, 891–908.

Merritt, J. L., Monsees, J. E., and Hendron, A. J. (1985). "Seismic design of underground structures." *Proc., 1985 Rapid Excavation Tunneling Conf.*, Vol 1, 104–131.

Minoura, Y., and Kamagata, K. (1964). "Stress relaxation of raw natural rubber." *J. Appl. Polym. Sci.*, 7, 1,077–1,087.

Mylonakis, G. (1995). "Contributions to static and seismic analysis of piles and pile-supported bridge piers." Ph.D. thesis, SUNY at Buffalo, N.Y.

Mylonakis, G., Syngros, C., Gazetas, G., and Tazoh, T. (2006). "The role of soil in the collapse of 18 piers of Hanshin Expressway in the Kobe earthquake." *Earthquake Eng. Struct. Dyn.*, 35, 525–545.

Nakamura, S., Yoshida, N., and Iwatate, T. (1996a). "Damage to Daikai subway station during the 1995 Hyogoken-Nambu earthquake and its investigation." *Proc., Japan Society of Civil Engineers*, Committee of Earthquake Engineering, 287–295.

Nakamura, Y., Uehan, F., and Inoue, H. (1996b). "Waveform and its analysis of the 1995 Hyogo-Ken-Nanbu Earthquake (II)." Railway Technical Research Institute.

Newmark, N. M. (1968). "Problems in wave propagation in soil and rock." *Proc., Int. Symp. on Wave Propagation and Dynamic Properties of Earth Materials*, Univ. of New Mexico, 7–26.

Okamoto, S. (1984). *Introduction to earthquake engineering*, 2nd Ed., Tokyo University Press, Tokyo.

O'Rourke, M. J., Bloom, M. C., and Dobry, R. (1982). "Apparent propagation velocity of body waves." *Earthquake Eng. Struct. Dyn.*, 10, 283–294.

Owen, G. N., and Scholl, R. E. (1981). "Earthquake engineering of large underground structures." *Rep. No. FHWA/RD-80/195*, Federal Highway Administration and National Science Foundation, Washington, D.C.

PB. (1991). "Trans-Bay tube seismic joints post-earthquake evaluation." *Rep. Prepared for the Bay Area Rapid Transit District*, Parsons, Brinckerhoff, Quade, and Douglas Inc.

Penzien, J. (2000). "Sresses in linings of bored tunnels." *Earthquake Eng. Struct. Dyn.*, 27, 283–300.

Penzien, J., and Wu, C. (1998). "Seismically-induced racking of tunnel linings." *Earthquake Eng. Struct. Dyn.*, 29, 683–691.

Poulos, H. G., and Davis, E. H. (1974). *Elastic solutions for soil and rock mechanics*, Wiley, New York.

Power, M. S., Rosidi, D., and Kaneshiro, J. (1996). "Vol. III: Screening, evaluation, and retrofit design of tunnels." *Research Rep.*, National Center for Earthquake Engineering Research, State Univ. of New York, Buffalo.

Rigo, A., et al. (1996). "A microseismic study in the western part of the Gulf of Corinth: Implications for large-scale normal faulting mechanisms." *Geophys. J. Int.*, 126, 663–688.

Sakurai, A., and Takahashi, T. (1969). "Dynamic stresses of underground pipeline during earthquakes." *Proc., 4th World Conf. on Earthquake Engineering*.

Schnabel, P. B., Lysmer, J., and Seed, B. H. (1972). "SHAKE—A computer program for earthquake response analysis of horizontally layered sites." *Report No. EERC 72/12*, Univ. of California, Berkeley, Calif.

Sextos, A., Kappos, A., and Pitilakis, K. (2003a). "Inelastic dynamic analysis of RC bridges accounting for spatial variability of ground motion, site effects, and soil-structure interaction phenomena. Part 2:

Parametric study." *Earthquake Eng. Struct. Dyn.*, 32, 629–652.
Sextos, A., Pitilakis, K., and Kappos, A. (2003b). "Inelastic dynamic analysis of RC bridges accounting for spatial variability of ground motion, site effects, and soil-structure interaction phenomena. Part 1: Methodology and analytical tools." *Earthquake Eng. Struct. Dyn.*, 32, 607–627.
Somerville, P. (2000). "Seismic hazard evaluation." *New Zealand Nat. Soc. Earthquake Eng. Bull*, 33(3), 371–386.
St. John, C. M., and Zahrah, T. F. (1987). "Aseismic design of underground structures." *Tunn. Undergr. Space Technol.*, 2(2), 165–197.
"State-of-the-art report." (1997). *Tunn. Undergr. Space Technol.*, 12(2), 83–355.
Stewart, J. P., et al. (2001). "Ground motion evaluation procedures for performance based design." *Rep. No. PEER-2001-09*, Pacific Earthquake Engineering Research Center, Univ. of California, Berkeley, Calif.
Trifunac, M. D., Todorovska, M. I., and Lee, V. W. (1998). "The Rinaldi strong motion accelerogram of the Northridge, California, earthquake of 17 January, 1994." *Earthquake Spectra*, 14(1), 225–239.
Tselentis, A., et al. (2004). "Estimation of seismic hazard and seismic deformation of the Rion-Antirrion straits." *Technical Rep. O.S.E.*, Earth Research Ltd.
Vrettos, C. (2005). "Design issues for immersed tunnel foundations." *Proc., 1st Greece–Japan Workshop on Seismic Design, Observation, and Retrofit of Foundations*, G. Gazetas, Y. Goto, and T. Tazoh, eds., 257–266.
Vucetic, M., and Dobry, R. (1991). "Effect of soil plasticity on cyclic response." *J. Geotech. Engrg.*, 117(1), 89–107.
Wang, J. N. (1993). "Seismic design of tunnels: A State-of-the-Art approach." *Monograph 7*, Parsons, Brinckerhoff, Quade, and Douglas Inc., New York.